https://doi.org/10.5194/egusphere-2025-6504
Preprint. Discussion started: 13 January 2026

The Diagenetic Fingerprint of Rotliegend Sandstones in the Groningen Gas Field

Sebastian J. Mulder[1*], Marita Felder[2], Johannes M. Miocic[1]

[1]*Energy and Sustainability Research Institute Groningen, Faculty of Science and Engineering, University of Groningen, Nijenborgh 6, 9746AG Groningen, the Netherlands*

[2]*Molenaar GeoConsulting, Richard Wagnerlaan 11, 2253CA Voorschoten, The Netherlands*

Corresponding author: Sebastian J. Mulder (sebastianmulder32@gmail.com)

Abstract

Permian Rotliegend sandstones form the main reservoir of the Groningen gas field, where reservoir quality is strongly influenced by diagenesis. This study presents the first field wide petrographic inventory of authigenic minerals, , their paragenesis, and spatial variations. Eodiagenesis under arid conditions formed hematite, clay coatings, and pervasive dolomite and anhydrite cements that stabilized the framework but reduced porosity. Mesodiagenesis involved feldspar dissolution and the precipitation of kaolinite, illite, chlorite, and limited quartz cement, with quartz growth commonly inhibited by clay coatings. Illite and chlorite are more abundant in northern playa margin facies, while kaolinite prevails in the south and is linked to feldspar alteration. Later uplift and reburial contributed little additional cementation and gas charge likely restricted large-scale fluid flow, limiting further cementation while localized influx from overlying and underlying strata may have occurred. Early dolomite was the most significant dominant porosity-reducing phase, whereas radial illite was volumetrically minor and had little impact. Overall, reservoir quality reflects the interplay of depositional environment, burial conditions, and local diagenetic processes. The results provide a framework for predicting spatial heterogeneity and assessing reservoir performance in Rotliegend sandstones.

Keywords

Rotliegend sandstones, Groningen gas field, authigenic minerals, diagenesis, clay coatings

1. Introduction

The Groningen gas field, situated in the northeastern Netherlands, is Europe's largest onshore gas accumulation. Approximately 75% of its original 2,800 billion cubic meters of recoverable gas has been produced from the Upper Permian Rotliegend sandstone reservoir before its closure in 2023 (Gast et al., 2010; Smith et al., 2019). Decades of gas extraction have induced surface subsidence and seismicity in the region (van Thienen-Visser et al., 2015; Postma and Jansen, 2018; Verberne et al., 2021), stimulating renewed interest in the geological factors that influence reservoir behavior. A thorough understanding of compaction and deformation requires detailed knowledge of the mineralogical framework and diagenetic evolution of the Rotliegend sandstones. In particular, the occurrence and distribution of authigenic minerals exert a first-order control on reservoir properties through their impact on porosity and permeability. Establishing the types and origins of these authigenic phases is therefore a necessary step towards linking petrographic and diagenetic variability with reservoir's diagenetic framework and mechanical behavior.

Mechanical and chemical properties of sandstones are strongly controlled by diagenetic reactions occurring during burial, either enhancing or degrading reservoir quality (Paxton et al., 2002; Worden and Burley, 2003; Becker et al., 2017; Busch et al., 2017; Worden et al., 2018). Diagenetic processes progressively alter the pore network through physical compaction and chemical reactions including cementation, dissolution, and recrystallization (Gaupp et al., 1993; Burley and Worden, 2003). The final reservoir quality is determined by the balance between porosity-destroying processes (e.g., cementation, chemical compaction) and porosity-preserving processes (e.g., dissolution, inhibition of cementation) (Worden and Morad, 2003; Ajdukiewicz et al., 2010; Busch et al., 2020). Furthermore, the

https://doi.org/10.5194/egusphere-2025-6504
Preprint. Discussion started: 13 January 2026

mineralogical and petrophysical properties of a sandstone are a function of its provenance, depositional environment, and diagenetic history. The diagenetic overprint is controlled by internal factors such as initial sediment composition and texture, and by external factors including burial history (e.g., maximum depth, temperature) and regional processes like uplift and/or fluid flow (Sindern et al., 2019; Griffioen et al., 2025). As burial progresses, the interplay of these diagenetic reactions becomes increasingly complex, and their cumulative impact is reflected in the wide variability of reservoir properties observed across siliciclastic reservoir rocks (Morad et al., 2010; Taylor et al., 2010; Worden et al., 2018).

Shortly after deposition, sandstones undergo early diagenetic reactions (eodiagenesis) that establish the framework for later burial history. In the Rotliegend sandstones of the Southern Permian Basin (SPB), as in other continental sandstones, these include clay infiltration and coatings, early carbonate and evaporite cements, and calcrete-dolocrete formation in paleosols (Glennie et al., 1978; Purvis, 1992; Platt, 1994; Ehrenberg, 1993; Morad et al., 2000; Molenaar and Felder, 2018). Clay coatings (illite, chlorite, smectite) are particularly significant: whether derived from mechanical infiltration or direct precipitation, even thin rims can inhibit quartz overgrowth nucleation and help preserve porosity to burial depths >4 km (Heald and Larese, 1974; Bloch et al., 2002; Ajdukiewicz et al., 2010; Ajdukiewicz and Larese, 2012; Busch et al., 2017). During mesodiagenesis (>70 °C, >2 km), precursor clays such as smectite typically transform into illite or chlorite, while these same coatings may enhance chemical compaction by promoting pressure solution and supplying silica for cementation (Sibley and Blatt, 1976; Aagaard et al., 2000; Walderhaug and Bjørkum, 2003; Busch et al., 2017). Early pore-lining dolomite rhombs represent the first widespread carbonate cement in the Rotliegend, followed by ferroan dolomite and later authigenic quartz, dolomite, illite, chlorite, and kaolinite (Gaupp et al., 1993; Amthor and Okkerman, 1998; Gluyas and Leonard, 1995; Ziegler, 2006; Gaupp and Okkerman, 2011; Griffioen et al., 2025). While such cements can occlude pores, they may also stabilize the framework against early mechanical compaction, when porosity and permeability are otherwise rapidly lost by grain rearrangement and deformation as fluids are expelled or trapped under overpressure (Paxton et al., 2002; Worden and Morad, 2003; Busch et al., 2024; Griffioen et al., 2025).

To date, no comprehensive study has systematically examined the relationship between petrography, diagenesis, and reservoir properties at the scale of the Groningen gas field and the adjacent Annerveen and Langebrug fields. The present study therefore aims to (1) characterize the detrital composition, (2) document the types of authigenic minerals present in the reservoir, and (3) determine the origin of cements and the mechanisms that control their distribution. Together, these objectives allow the construction of a diagenetic model that links depositional facies, diagenetic pathways, and reservoir properties. By integrating data from over 300 thin sections from 15 wells across the field, this study provides a comprehensive view of diagenetic variability and its controls, offering new insights into the interplay between authigenic mineral assemblages and depositional environments.

2. Geological Setting

The Rotliegend sandstones of the Groningen field as well as of the Langebrug and Annerveen fields are located on the southern margin of the SPB (Fig. 1A), a sedimentary basin stretching from the United Kingdom to the Baltic states. The sandstone deposits overly the Stephanian deposits from the Carboniferous, which are divided by the Base Permian Unconformity (Veen et al., 2025). During the Permian, the region experienced an arid climate, with sediment supply influenced by the Variscan orogen and London–Brabant Massif, tectonic subsidence, and climatic variation (de Jager, 2007; Geluk, 2007; Gast et al., 2010). In the Netherlands, the Rotliegend sediments are subdivided into the Lower Rotliegend and the Upper Rotliegend. The Lower Rotliegend comprises volcanic and clastic deposits of limited extent above the Base Permian Unconformity (Veen et al., 2025). In contrast, the Upper Rotliegend is primarily represented by the Slochteren Formation (Fig. 1B-C), a series of fluvial and aeolian sandstones interbedded with mudflat and playa shales. The Slochteren sandstones are

https://doi.org/10.5194/egusphere-2025-6504
Preprint. Discussion started: 13 January 2026

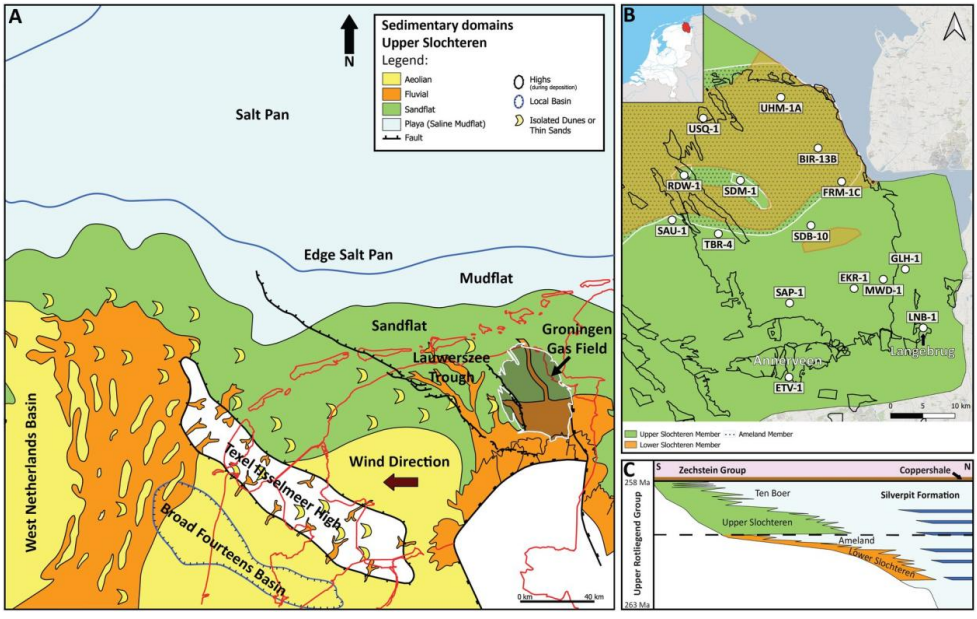

Figure 1: The Upper Rotliegend Group in the Dutch part of the SPB and the Groningen area. A) Map with the depositional environments of the Upper Slochteren interval in the Netherlands, structural elements, and the location of the Groningen gas field. Modified after Fryberger et al. (2011). B) Map of the Groningen area with well locations of this study, and the different units of the Slochteren Formation and Silverpit Formation. The formation maps are from TNO-GDN (2025). The outlines of the different gas fields are shown in black. C) The regional chronostratigraphic scheme of the Groningen area. Modified after Henares et al. (2014).

stratigraphically subdivided by shale deposits of the Ameland and Ten Boer members (Geluk, 2007; Veen et al., 2025). Both represent transgressive phases of the Silverpit Formation, which thickens further north in the SPB (Nicholls et al., 1987). The Ameland Member, which separates the Lower and Upper Slochteren Members, is characterized by finer-grained clay-rich deposits and terminates towards the south (Fig. 1B-C). The Lower Slochteren and Ameland Members are absent in the north near Stedum-1 (SDM-1) and Rodewolt-1 (RDW-1) (Fig. 1B). Overlying the Upper Slochteren, the Ten Boer Member is dominated by siltstones and mudstones as part of the Silverpit Formation (Geluk, 2007; Gast et al., 2010). Overall, the SPB was an underfilled, slowly subsiding basin where accommodation exceeded sediment supply (de Jager and Visser, 2017).

The Slochteren Formation in the Groningen gas field represents a complex depositional system characterized by a large-scale S-N proximal-to-distal trend. This trend transitions from pebbly and conglomeratic lithofacies in the south, through clean sandstones in the central part of the field, to clay-rich facies in the north. Its sedimentary environments include braided fluvial systems, aeolian sandflat and minor dune deposits, and floodplain to playa deposits, reflecting dynamic environmental changes (Gast et al., 2010). The stratigraphic changes of the facies belts are controlled by tectonics, by climate, and by related lake-level fluctuations. Southward, towards the Annerveen and Langebrug fields, conglomerates and pebbly sandstones increase in content, with the Langebrug field characterized by a thicker Ten Boer mudstone interval compared to the Annerveen field. Conversely, northward of the Groningen gas field, sandstone intervals progressively pinch out, transitioning into claystone and evaporitic salts (de Jager and Visser, 2017).

The Groningen reservoir spans an area of approximately 862 km² (Fig. 1B), with thicknesses ranging from 70 meters in the south to over 240 meters in the north (van Thienen-Visser and Breunese, 2015), reflecting the base Permian relief. High porosity sandflat and fluvial deposits dominate the central part

https://doi.org/10.5194/egusphere-2025-6504
Preprint. Discussion started: 13 January 2026

of the field, transitioning to fluvial and clay-rich facies towards the south and north, respectively. The change in sedimentary facies significantly impacts reservoir quality (Nicholls et al., 1987; de Jager and Visser, 2017). Continuous wind reworking of the fluvial sediments redistributed available sediment in the Groningen area and towards the Lauwerszee Trough (Fig. 1A), where mainly aeolian deposits accumulated due to prevailing easterly winds. These local physiographic conditions strongly influenced lithofacies distribution, resulting in well-sorted sediments despite variations in sedimentary structures.

The high porosity and permeability of the Groningen reservoir are partially attributed to to the well-sorted nature of the sandstones, although these properties are not uniform across the field. Minor intercalations of finer- and coarser-grained sediments had little effect on average porosity (de Jager and Visser, 2017). Another important factor controlling the reservoir quality is burial diagenesis, including compaction and cementation, which created significant heterogeneity in reservoir properties of the Slochteren sandstones (Geluk, 2007; Gaupp and Okkerman, 2011). Following deposition, the reservoir underwent substantial burial, reaching maximum depths of nearly 3500m in the north of the field and approximately 3000m in the south during the Middle Jurassic (Goldberg et al., 2017; Bouroullec et al., 2019; Amberg et al., 2022). Toward the Late Jurassic, the Groningen area experienced uplift to an average depth of 1500m during which preexisting faults in the Rotliegend were reactivated and the current structural setting of the gas field was formed (Ziegler, 1975; Kortekaas and Jaarsma, 2017; de Jager and Visser, 2017). Initial hydrocarbon charge of the Rotliegend reservoir, due to expulsion of hydrocarbon-bearing fluids from underlying Carboniferous strata is interpreted to have occurred prior to the major Late Jurassic uplift phase (Lee et al., 1985; Sissingh, 2004; de Jager, 2007; Clauer et al., 2012). Subsequent uplift likely arrested gas charge until reburial re-initiated hydrocarbon generation by achieving thermal maturity at greater depths (de Jager et al., 1996; Gaupp and Okkerman, 2011; Remmelts et al., 2025). During the Late Cretaceous and Tertiary periods, the reservoir was reburied to depths of 2600–3300 m in the Groningen and Annerveen fields and 3735 m in the Langebrug field, accompanied by fault reactivation related to Alpine inversion (Kortekaas and Jaarsma, 2017).

3. Methodology

3.1 Sample Selection

Core samples were selected from 15 wells from the Upper Rotliegend Slochteren interval in three north-south profiles spanning the entire Groningen reservoir, and the Annerveen and Langebrug reservoirs (Fig. 1B). The depth of the cored intervals ranges between 2600m and 3300m true vertical depth (TVD) with the exception of one core from the Langebrug reservoir that has an average depth of 3735m. From each core, 25–35 core plugs were sampled to represent the entire Rotliegend sandstone interval, including siltstones, and mudstones (Table 1). Sampling targeted various lithofacies to include the diversity of depositional environments present within the cores. To minimize sampling bias, consistent depth intervals were maintained. Additionally, 2–3 plugs were selected from the Ten Boer Member and Ameland Member, if present within the core.

3.2 Petrographic Analysis

Petrographic analysis was performed on a total of 310 thin sections to assess texture, detrital composition, authigenic cements, and porosity. Thin sections where cut from epoxy-impregnated core plugs to enhance pore visibility under an optical microscope. Sandstone composition was systematically point-counted based on 300 points per thin section using a Petrog point count stage to quantify detrital grains, authigenic minerals, and pore type. Image acquisition during point counting was conducted with a Leica DM2700 P microscope equipped with a Leica DMC5400 digital camera and controlled by LAS X software (University of Groningen), which facilitated additional documentation of compositional and textural properties. Furthermore, all thin sections were scanned using a Zeiss Axio Scan Z1 Slide Scanner (Utrecht University) to produce high-resolution digital images. The scanner captured images

https://doi.org/10.5194/egusphere-2025-6504
Preprint. Discussion started: 13 January 2026

at 10× magnification in both plane-polarized light (PPL) and cross-polarized light (XPL) at six different rotational angles (0°, 15°, 30°, 60°, and 75°).

3.3 Scanning Electron Microscopy

Scanning Electron Microscopy (SEM) was applied on 31 selected samples to examine mineralogical textures, authigenic cements, pore morphology, and diagenetic features at a smaller scale than optical microscopy. SEM imaging was performed on 18 polished thin sections using a Zeiss Evo 15 with high-definition backscattered detection (HDBSD) and Energy Dispersive X-ray (EDX) spectroscopy for quantitative elemental mapping. These analyses facilitated the classification of authigenic and detrital minerals and provided insights into the diagenetic evolution and distribution of authigenic clays in the intergranular and intragranular pore space. Subsequently, high-resolution 3D SEM imaging was conducted on 13 uncoated, freshly broken surfaces of plug counterparts using a Zeiss Gemini 450 with secondary electron (SE2) detection. This approach provided detailed morphological characterization of the different authigenic minerals, offering complementary data to the two-dimensional analyses from thin sections.

3.4 Statistical analysis of point count data

Point count data of the authigenic minerals have been analyzed using Correspondence Analysis (CA) to explore relationships between mineral distributions across the wells. This method provides a statistical approach to identifying compositional trends and associations within the dataset, offering insights into diagenetic processes and spatial variability. CA is a multivariate statistical method designed to explore relationships within categorical datasets by transforming contingency tables into a lower-dimensional space (Greenacre, 2017). It is particularly useful for geochemical and mineralogical studies where variables are represented as proportions rather than absolute quantities (Davis, 2002; Rosera and Coleman, 2021). CA operates using a chi-square distance metric, ensuring that compositional data is analyzed while preserving relative abundances. The method involves normalizing the dataset into a row-profile matrix, where each row represents a sample and each column represents a mineral category. Singular Value Decomposition (SVD) is then applied to extract latent dimensions, which capture the primary gradients of variation in the dataset. The resulting biplot displays wells and minerals within the same coordinate system, facilitating the interpretation of mineralogical associations. The theoretical background for this approach follows the framework established by Greenacre (2017), which provides a foundation for the application and interpretation of CA in various scientific fields (Rosera and Coleman, 2021).

4.1. Detrital composition

The sandstones of the Slochteren Formation can generally be classified as sublitharenites, and lithic subarkoses, showing a relatively low variability in detrital composition (Tab. 1, Fig. 2). Quartz (50-75%) dominates the detrital framework, occurring primarily as monocrystalline and polycrystalline grains, with the latter often having metamorphic origins. Feldspars are the least abundant (0-17%) relatively to the other detrital grains and include microcline and albite. The lithic fragments (2-40%) consist predominantly of metamorphic and volcanic fragments. The metamorphic fragments comprise quartz-mica schists, gneiss, phyllites and altered and undifferentiated grains. Volcanic lithics consist of devitrified volcanic glass and felsic crystalline fragments. The sedimentary rock fragments can be subdivided in intrabasinal and extrabasinal clasts and comprisechert, mudclasts, siltstones, sandstones, carbonate, and anhydrite grains, respectively. Carbonate intraclasts are uncommon but occur throughout the field, especially in the Ten Boer Formation of northeastern wells and in fluvial sandstones of the Annerveen and Langebrug reservoirs (Fig. 3A–B). Some are composed of dolomite intergrown with anhydrite, while others are as dolomite-siliciclastic grains intergrown with detrital clay (Fig. S1A-D). In the Annerveen and Langebrug reservoirs, carbonate intraclasts are more prevalent, appearing as

https://doi.org/10.5194/egusphere-2025-6504
Preprint. Discussion started: 13 January 2026

Table 1: Average composition of detrital and authigenic minerals, alongside the core lithology, for the studied cores.

	Well Names		ETV-1	LNB-1	SAP-1	EKR-1	MWD-1	GLH-1	TBR-4	SDB-10	SAU-1	FRM-1C	SDM-1	RDW-1	BIR-13B*	USQ-1	UHM-1A
	Geographic location		South						Middle					North			
	Core top (m)**		3174	3824.0	2750	2653.6	2778	3106	2752	2863	3474	3827	2845	3140	3778	2902	2930
	Core bottom (m)**		3312.3	3867.9	2898.9	2738.5	2913	3124	2993	2930.5	3529.2	4049.1	3072.36	3180.5	4040.02	3210.5	3164.5
	Cored material RO (m)		138.3	43.9	148.9	84.91	135	18	247	67.5	55.16	222.1	227.36	40.5	262.02	308.5	234.5
	Cored members (m)	ROCLT	7.5	21.5	26.5	n.a.	33.454	n.a.	84.45	n.a.	n.a.	18.6	17.2	n.a.	71	70	16.51
		ROCLA	n.a.	n.a.	n.a	n.a.	n.a.	n.a.	n.a.	n.a	n.a	12	n.a.	n.a.	11.28	12.5	21.75
	Amount of samples		24	12	26	19	23	8	26	20	10	26	25	16	21	27	26
	Grain size (µm)		342.0	407.9	264.4	269.1	254.3	301.2	285.0	232.0	255.6	232.0	231.9	236.4	168.1	211.5	206.9
	Quartz		60.7	45.7	56.0	58.4	55.5	55.1	57.1	59.9	58.1	57.1	55.8	57.6	46.8	54.5	59.7
	Feldspar		2.5	1.9	1.9	4.1	6.2	6.2	3.6	5.5	6.4	6.1	4.2	4.9	6.5	5.4	3.9
Detrital	Lithics		10.9	17.3	10.9	11.8	13.3	13.8	10.2	10.8	12.2	11.1	10.8	10.9	8.3	8.8	8.9
	Accessories		0.8	1.2	0.5	0.6	0.4	0.3	0.4	0.4	0.4	0.3	0.5	0.4	0.7	0.8	0.6
	Clay matrix		1.4	8.8	3.3	1.0	1.8	0.4	3.2	0.8	0.4	3.8	1.3	0.2	14.1	7.5	1.7
	Clay cutans		0.3	2.4	0.1	0.1	0	0.2	0.1	0.2	3.3	0.8	0.3	0.2	0.1	1.1	0.5
	Tangential illite		0.7	0.9	0.7	1.3	0.8	2.1	1.0	1.2	2.5	2.7	1.8	2.9	2.7	1.9	1.9
	Radial and meshwork illite		0	0.3	0	0	0	0.7	0.1	0.0	1.0	0.1	0.1	0.2	0.5	0.2	1.0
	Chlorite		0	0.3	0.1	0.2	0	0.4	0.1	0	0.6	0.4	0.2	0.3	0.2	0.8	0.8
Authigenic	Illite-smectite		0.4	0.8	0.7	0.5	1.3	1.1	1.4	0.6	0.4	1.8	0.7	2.4	1.5	1.7	1.8
	Kaolinite		1.7	0	4.1	3.1	2.9	1.4	2.6	3.5	1.3	0.7	4.4	4.2	1.2	0.8	0.7
	Dolomite		12.7	15.8	15.4	11.3	8.1	9.8	11.6	7.9	4.7	8.7	12.0	7.4	10.2	7.9	9.8
	Quartz		2.6	1.9	1.4	1.8	1.4	1.2	0.9	0.5	1.3	0.9	0.5	1.1	0.7	1.6	1.5
	Anhydrite		0.6	0.3	0	0	0.1	0.1	0.3	0	0	0	0	0	1.3	0.9	0
	Barite		0.1	0.1	0.4	0.1	0.1	0	0.2	0.2	0	0.1	0.1	0.1	0.5	0.2	0.2
	Intergranular porosity		3.7	0.6	2.9	4.8	7.7	4.6	5.1	7.5	4.7	4.7	6.1	4.6	4.0	4.1	6.4
	Intragranular porosity		0.9	1.6	1.4	0.8	0.4	2.6	2.4	1.0	2.6	0.7	1.3	2.8	0.8	1.6	0.6

* Large inclination and, therefore, a lot of Ten Boer Member core material
** Measured Depth (m) below sea-level

larger, pebble-sized grains within the sand matrix. Some of these carbonate intraclasts are covered with inherited hematite rich clay coatings in some of the samples (Fig. 3A-B). Accessories include mica (biotite, muscovite), heavy minerals (e.g., zircon, tourmaline), and opaques. The sandstones also contain incomplete tangential clay coatings (Fig. 3C–E), thickest in grain embayments and absent where abraded (Fig. 3F). The coatings consist of smectite and iron oxides, with minor carbonate and anhydrite microcrystals, and their color varies from dark brown to reddish depending on hematite content (Fig. 3F).

4.2 Authigenic mineralogy

Authigenic mineralogy within the Rotliegend sandstone reservoir of the Groningen Gas Field comprises a wide variety in authigenic minerals occurring as intergranular pore-fill, grain-coating, and replacement materials. Authigenic minerals in the studied thin sections include clay cements, such as illite, illite-smectite, chlorite and kaolinite. Cements, in decreasing abundance, include dolomite, Fe-dolomite, quartz, and sulfates such as anhydrite and barite. Illite is the most widespread clay cement, occurring as grain coatings, while dolomite and quartz dominate as intergranular pore-filling cements. Anhydrite and barite occur as anhedral to euhedral cements, often in localized concentrations. The distribution and extent of these cements varies throughout the field.

4.2.1 Mixed authigenic clay and Illite

Mixed authigenic clay, as described in this study, is generally present as tangential illite-smectite clay coatings and as illite-smectite intergranular cement, with locally minor amounts of chlorite. Authigenic illite in the Groningen area is observed in all wells and increases from less than 1% in the south to 9% in the north. It is primarily present as intergranular rim cement typically occurring around detrital grains and often following the distribution pattern of pre-existing tangential clay coatings (Fig. 3C). The mineral has a variety of different morphologies. In the intergranular pore space, three different morphologies are observed in the form of tangential, radial and meshwork illite in the intergranular pore space (Fig. 3C-F; Fig. 4A-C), while bladed illite is observed within dissolved grains (Fig. 4D).

https://doi.org/10.5194/egusphere-2025-6504
Preprint. Discussion started: 13 January 2026

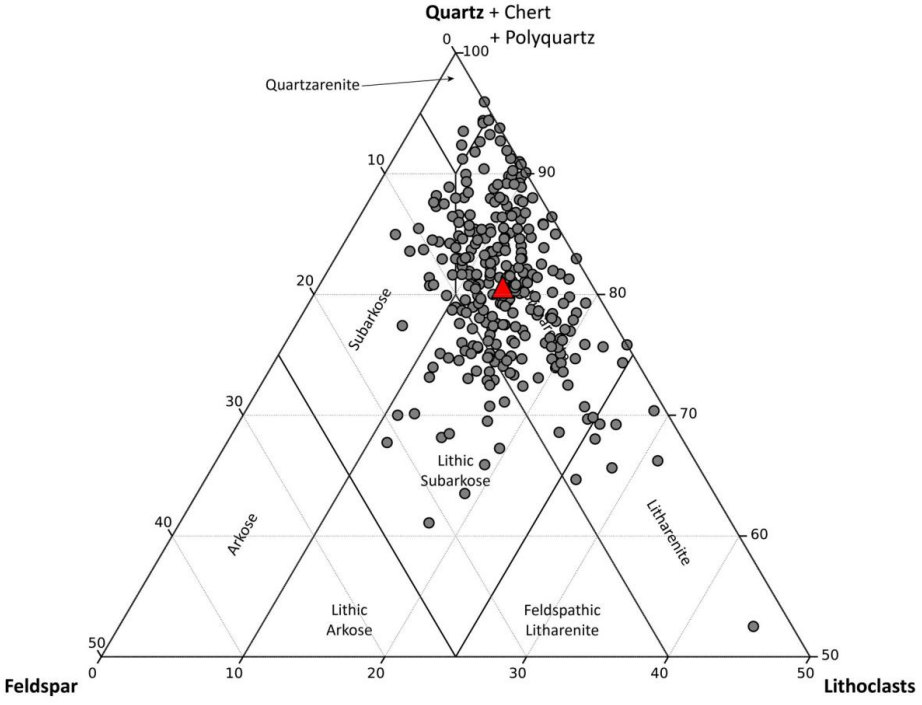

Figure 2: QFL ternary diagram showing the present-day sandstone composition of the studied samples of the Groningen area (after Pettijohn et al., 1975). The composition is based on point count data (N=310) recalculated to represent QFL percentages. The red marker displays the mean composition of the sandstone samples, which are generally classified as sublitharenites.

Tangential illite coatings

Tangential illite coatings commonly occur directly on detrital grains and are characterized by thin and well-aligned layers of clay plates oriented parallel to detrital grain surfaces. This illite is usually intermixed with varying amounts of illite-smectite. Under optical microscopy, tangential illite occurs in two varieties: dark red hematite-stained thick clay coatings and colorless thin coatings of which the latter is characterized by yellow-to-blue birefringence colors in cross-polarized light (Fig. 3D). These coatings often vary in thickness, ranging from a single clay plate to multi-layered micro-laminated sheets. In SEM images, tangential illite appears as thin, platy ('flaky') crystals oriented parallel to grain surfaces. The red tangential clay coatings differ from the detrital incomplete coatings as they completely envelop grains and are formed in-situ. These coatings are common in in the Langebrug reservoir and in a few other wells (SAU-1, USQ-1). The colorless tangential illite commonly covers the red tangential coatings. Both tangential illite coating types are often present at point, and long grain-to-grain contacts, although thinner and not fully developed into crystalline illite (Fig.3F). Their presence at grain-to-grain contacts is evidence for a pre-compactional formation and their thinning indicates that they were compacted at the grain-to-grain contacts. The tangential illite coatings increase in content towards the northeastern part of the field in finer grained sandstones (Table 1).

https://doi.org/10.5194/egusphere-2025-6504
Preprint. Discussion started: 13 January 2026

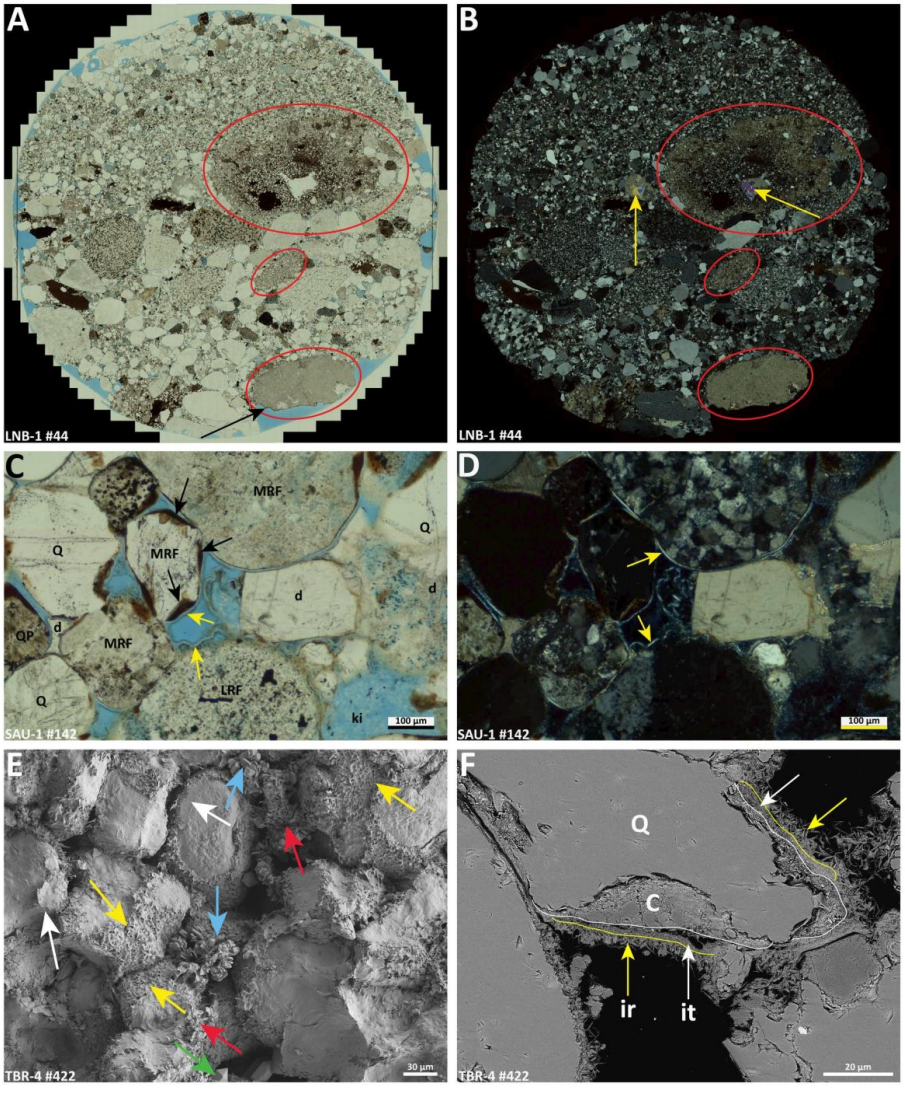

Figure 3: Detrital dolomite intraclasts, detrital clay rims, and different types of authigenic illite in the Rotliegend sandstones. Detrital grains are Monocrystalline quartz (Q), Polycrystalline quartz (QP), (Leached) Feldspar (LF), Plagioclase (FP), Metamorphic rock fragments (MRF), (Leached) rock fragments (LRF). A-B) Large dolomite grains in a poorly sorted coarse grained fluvial deposit (red circles). The nature of the grain is obscured by compaction and carbonate overgrowths, although hematite rims (black arrow) indicate the detrital origin. The dolomite grains consist of dolomite rhombs in clay matrix, small rhombs or fine framework grains supported by dolomite cement. Locally, the grains contain anhydrite cement (yellow arrows). The diameter of the thin section is 2.5 cm. C-D) Cutans (black arrows) and radial (fibrous) illite (yellow arrows) perpendicular on incomplete inherited red clay rims. Note the high birefringence colors of the radial illite in the XPL image. Dolomite (d) formed after radial illite and Intragranular kaolinite (ki) is present in a dissolved feldspar grain. E) 3D SEM image showing cutans and post burial authigenic illite cement rims and pore-filling illite cements in the sandstones. 'Honeycomb' illite (yellow arrows) is typically formed on tangential illite (white arrows). Locally, fibrous 'meshwork' illite has formed between kaolinite booklets (red arrows). Kaolinite (or dickite) fills the pore space between the grains (blue arrows). Euhedral quartz cement (green arrows) fills the pore space as well. F) In-situ formed illite cutans (it; white arrows) on inherited clay cutans (C). The latter only covers grain embayments in detrital quartz grains. Radial illite (ir; yellow arrows) has formed as a subsequent phase on the tangential illite. Note that the tangential illite is partially separated from the tangential illite

https://doi.org/10.5194/egusphere-2025-6504
Preprint. Discussion started: 13 January 2026

Radial and meshwork illite

On top of tangential coatings, authigenic illite grew outward as radially oriented platy crystals, arranged in honeycomb or boxwork patterns around grains (Fig. 3E; Fig. 4A) or as thin fibrous illite. This general textural class is termed radial illite. here called as radial illite (Fig. 4B). Crystals range 2–15 µm in length and 0.4-0.9 µm in thickness, with radial illite containing significant microporosity. Radial illite is less uniformly arranged than tangential rims, giving a heterogeneous texture (Fig. 3E–F). In some sandstones (e.g. wells MWD-1, USQ-1), the tangential and radial illite is detached from clay coatings (Fig. S1E) or preserved as a remnant rim of a dissolved grain. Locally, platy illite crystals are observed between the detached clay rim and the underlying grain or illite coating (Fig. 4A). In a few samples, fibrous illite also occurs between kaolinite booklets (Fig. 3E).

Where radial illite filaments intertwine across pores, the illite is defined as meshwork illite. It is present where there is sufficient pore space (Fig. 4A-B). In some samples, meshwork illite occurs in a loosely packed arrangement within interparticle pores, whereas in others, it forms denser, continuous pore-bridging layers. Radial and meshwork are slightly more prevalent in northeastern cores and is particularly abundant in wells UHM-1 and USQ-1, with somewhat higher amounts also in SAU-1.

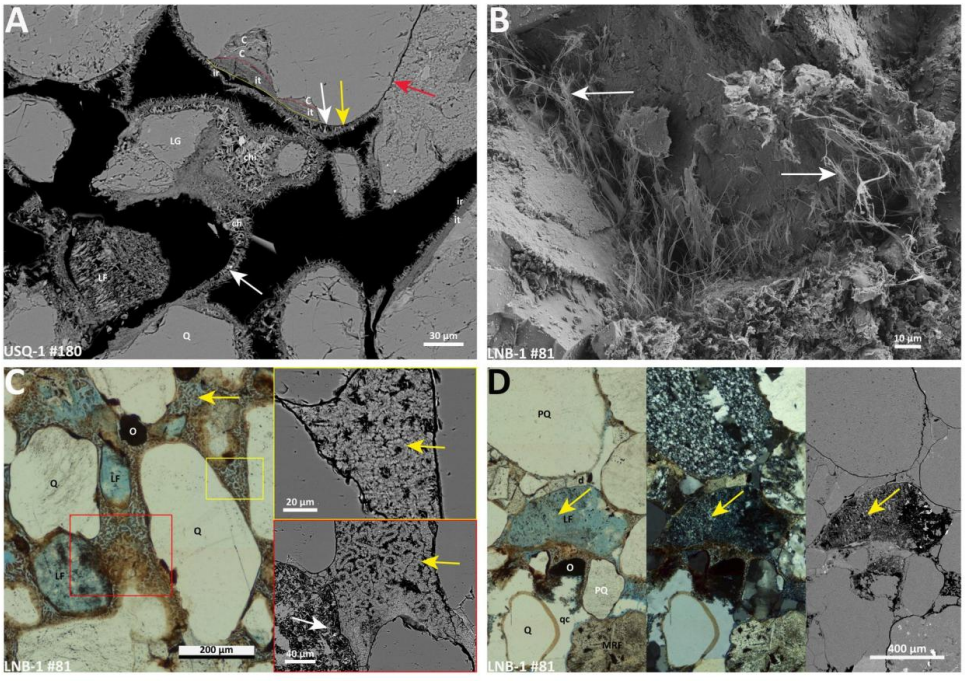

Figure 4: Radial, fibrous, and intragranular illite in the Rotliegend sandstones. A) Multiple phases of illite and chlorite cement in a northern core (USQ-1). Several generations of clay rims are highlighted by the colored lines. Two layers of inherited clay cutans in a grain embayment are covered by a succession of tangential and then radial illite. Furthermore, radial illite is observed between detached illite rims (yellow arrow), although it is absent from grain contacts (red arrow), indicating that it formed after subsequent burial and compaction. Chlorite (ch) can be observed as light colored crystals platelets between the radial illite rims (white arrows) and as intragranular cement (chi). B) 3D SEM image of extensive fibrous ('hairy') illite cement (white arrows), which fills intergranular pores and reduces them to micropores. This type of illite greatly reduces pore connectivity. C) Fibrous snake-like illite aggregate in a pore (yellow arrows). Quartz cement (qc) engulfs illite, hence formed after the illite. D) Intragranular illite follows the cleavage planes of a partially dissolved feldspar (LF) and forms 'ghost' structures (yellow arrow). Note that small opaque cement crystals formed in the dissolved grain as well.

https://doi.org/10.5194/egusphere-2025-6504
Preprint. Discussion started: 13 January 2026

However, the illite content is not consistently elevated in all sandstones with higher tangential illite content, and its distribution remains heterogeneous with depth. These three wells, largely positioned in the water leg, also show high radial and meshwork illite content in the gas leg (Fig. 3E-F; Table 1). Furthermore, meshwork illite appears as folded, vermicular features, either semi-detached from grains or as pore-filling clay in the Langebrug reservoir, forming on thin tangential substrates (Fig. 4C). Usually there is a sequential evolution from tangential to radial to meshwork illite. This creates complex illite fabrics that encapsulate and bridge detrital grains, with radial and meshwork illite particularly influencing pore structure.

Intragranular illite

Intragranular authigenic illite is mostly associated with the dissolution of detrital K-feldspar. Bladed illite typically fills voids within partial dissolved feldspar along cleavage planes. Subsequent grain dissolution resulted in intragranular pores, with illite typically preserving the original cleavage or twinning structure of the precursor feldspar. In some instances, illite forms a meshwork or maintains an alignment according to former feldspar grain features, leaving behind 'ghost' structures (Fig. 4D). Moreover, intragranular illite has also been observed locally in altered and dissolved lithics, predominantly in altered volcanic grains. In polymineralic lithic fragments, some dissolved feldspar minerals were replaced by kaolinite, while others were replaced by illite, resulting in their segregation within the same dissolved grains.

4.2.2 Chlorite

Chlorite is present in minor amounts within the studied samples (0-4%). It is typically associated with dissolved lithics and feldspar, and seldom as an intergranular mineral (Fig. 4A; Fig. 5A-C). In intragranular pores, chlorite occurs as single crystal platelets or partially fills the pore space, commonly forming distinctive chlorite rosettes. It predominantly occurs in fully dissolved grains or grows atop and within other replacive authigenic clays, such as illite. Notably, chlorite does not follow the cleavage planes of dissolved feldspar. In intergranular pores, chlorite is observed on top of tangential clay rims where it is composed of single platelets in minor amounts or as a fan-like arrangement of multiple stacked platelets (Fig. S1F). Locally, it also occurs as single platelets between mixed-layered tangential clay coatings, aligning with the orientation of platy illite. Furthermore, chlorite is observed in small pore spaces between detached tangential clay coatings and grain boundaries, often intercalating with radial illite (Fig. 4A). Chlorite rosette crystals are generally larger than radial illite crystals, with length ranging from 5 to 25 µm. The chlorite content varies across the reservoir, with a slight increase towards the northern part of the field in wells north of SDB-10 (Fig. 1; Table 1). There, chlorite occurs between intergranular illite and illite-smectite pore-filling clays (Fig. 5D).

4.2.3 Kaolinite

Kaolinite (0-11%) commonly is present in both primary, and in secondary moldic pore spaces, where any residual ghost structures of the former grains are absent. This suggests that kaolinite formed after major grain dissolution. It predominantly forms pseudohexagonal platelets arranged in vermicular or booklet-like aggregates, exhibiting characteristic worm-like or locally sheaf-like textures (Fig. 5E-H). These aggregates range from densely packed clusters to isolated platelets within intergranular pores. The distribution is notably uneven, with some pores being densely filled while adjacent pores containing only isolated crystals. In SEM it is visible that blocky hexagonal crystals are often intercalating with vermicular kaolinite, which suggests the presence of dickite (Fig. 3E; Fig. S2A-B). In some instances, the kaolinite forms continuous intergranular pore-filling networks that envelop other cementing minerals, such as quartz, and dolomite. Locally, it has been observed engulfing quartz or anhydrite cements (Fig. 5E). Within dissolved grains, kaolinite is present as thin, randomly oriented booklets (Fig. 3C; Fig. 5G). In a few specific samples from well SAP-1, sheaf-like kaolinite has been identified (Fig. 5G). Bitumen-stained kaolinite has been observed in two cores, in the Ten Boer Member

https://doi.org/10.5194/egusphere-2025-6504
Preprint. Discussion started: 13 January 2026

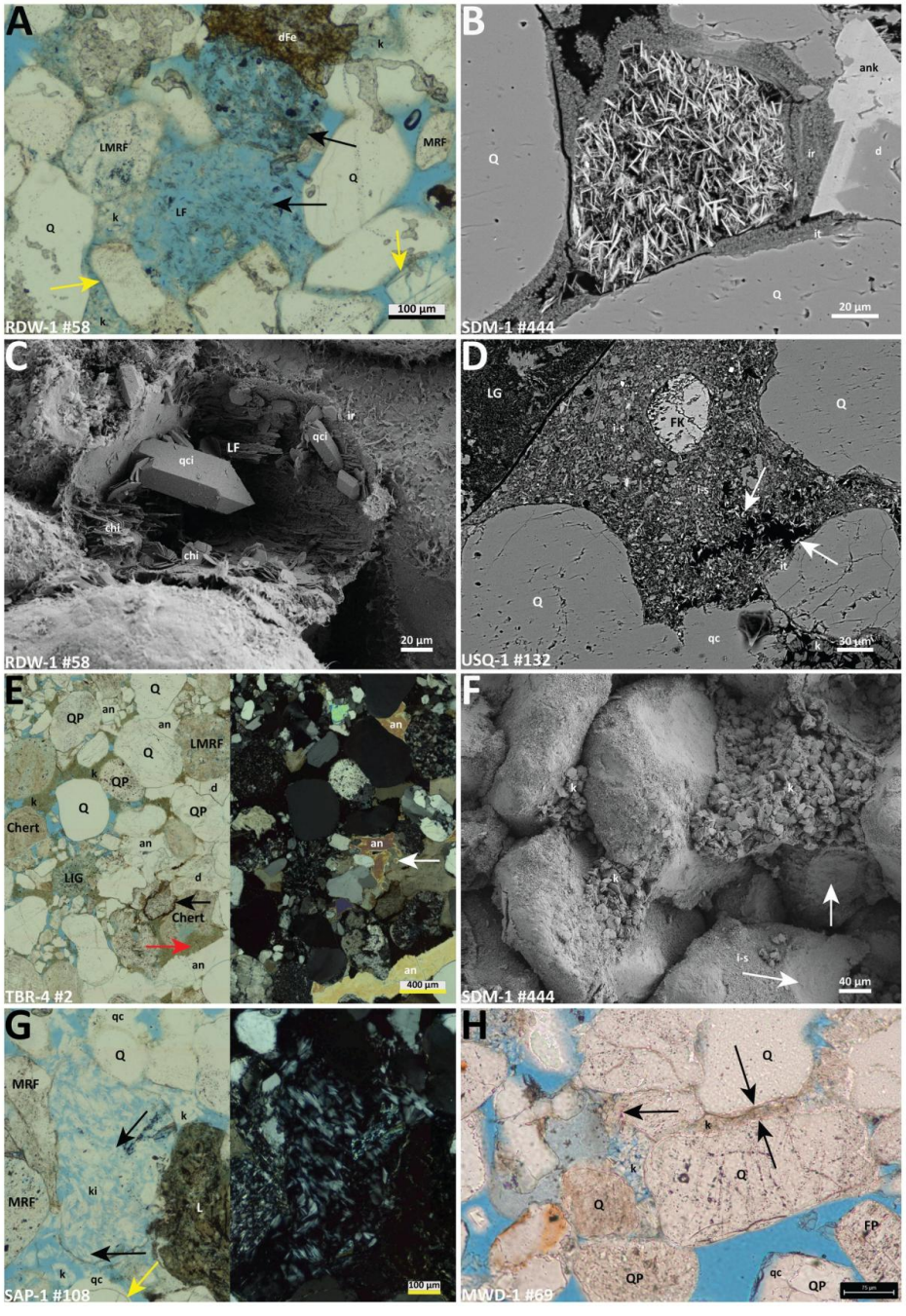

https://doi.org/10.5194/egusphere-2025-6504
Preprint. Discussion started: 13 January 2026

Figure 5: Different types of chlorite and kaolinite in Rotliegend sandstones. A) Intragranular chlorite platelets and rosettes (black arrows) that formed in a dissolved grain, which is typical for the sandstones in the Groningen gas field. The texture indicates that chlorite occurs in a former volcanic grain and likely replaces volcanic ash. Fe-Dolomite (dFe) follows the boundary of the dissolved grain. B) SEM image of intragranular chlorite platelets in a dissolved grain. Ankerite cement (ank) has formed as an overgrowth on a dolomite rhomb having a compromise boundary with the radial illite. C) 3D SEM image of a dissolved feldspar in which chlorite platelets and an euhedral quartz crystal (qci) formed on the inner rim. D) Pore-filling cement consisting of illite-smectite (i-s) and chlorite (white arrows), which is typical for wet sandflat sediments in the northern cores. A K-feldspar grain (FK) is floating in the microporous clay cement. E) Brown-stained slightly deformed kaolinite (k) is engulfed by anhydrite pore cement (an) as shown with the red arrow, which formed after partially dissolved dolomite cement (white arrow). Note the Fe-dolomite rim (black arrow) on the detrital dolomite grain. F) Aggregates of vermicular kaolinite booklets (k), which is typical for the Rotliegend sandstones. Note that crystallized illite-smectite clay rims are not present at former grain contacts (white arrows). G) Sheaf-like kaolinite (black arrows) in a dissolved grain. This type of kaolinite is only observed in the Sappemeer-1 (SAP-1) core. Note the hematite dust rim (yellow arrow) that separates the quartz overgrowth from the quartz grain. H) Densely packed kaolinite aggregate in the pore space between grains (black arrows).

of the TBR-4 well and in the Annerveen field (ETV-1 well), which provides further evidence of compositional variability across the region (Fig. 5E). Notably, kaolinite is absent in well LNB-1. In well MWD-1, densely packed kaolinite are locally observed where individual booklets appear compressed and reoriented, often aligning parallel to grain surfaces (Fig 5H).

4.2.4 Carbonate cement

Dolomite is the most pervasive cement among all authigenic minerals within the sandstones, ranging from sparse euhedral rhombs to a poikilotopic cement that can fully occupy the pore space of the sandstone samples (5-40%). The dolomite crystals vary in size (40-380 µm), and their distribution is often irregular, ranging from isolated crystal clusters to extensive intergranular pore-filling cements in others (Fig. 6A). Dolomite occurs in two primary forms: drusy cement and discrete rhombs. The drusy cement forms as a fine crystalline layer lining intergranular pore walls. In contrast, discrete dolomite rhombs are isolated, euhedral to subhedral crystals that are randomly distributed within the intergranular and intragranular pore space and in detrital grains. Dolomite rhombs commonly exhibit a poikilotopic texture, meaning that single crystals are encapsulating one or more detrital grains (Fig. 6B).

In clay matrix rich sandstones and mudstones, dolomite can reach contents of up to 40%, creating distinct zones of high cementation. In certain fine-grained sandstones and siltstones, dolomite cement is restricted to specific laminae where it fully occupies the pore space (Fig. 6C), while in coarser sandstones, extensive dolomite cementation is commonly found adjacent to mudstone contacts (Fig. 7). Furthermore, a dolomite supported fabric is prevalent in some of the poorly sorted fluvial sandstones of the Langebrug reservoir (LNB-1). Sandstones with a high content of dolomite cement often lack clay coatings around detrital grains (Fig. 6A, B, E). The early emplacement of this cement is evidenced by its profound inhibition of compaction. While non-cemented intervals are characterized by point, long, and occasional concavo-convex contacts, dolomite-rich sandstones retain floating grain textures with a complete absence of grain-to-grain contacts (Fig. 6B, Fig. 7B). The degree of compaction within these dolomite-cemented zones varies across the field, with some samples showing point contacts and others lacking them entirely, a variability that is consistent with the presence of more than one dolomite cement phase (Fig. 6A, E). Furthermore, local deformation of dolomite rhombs between rigid detrital grains indicates syn-compactional formation (Fig. 6D). Dolomite rhombs extend from intergranular pores into intragranular spaces (Fig. 6E). Within intragranular spaces, dolomite typically forms euhedral rhombs, either floating within partially dissolved grains or completely filling the intragranular pore space, making it difficult to distinguish authigenic dolomite from detrital carbonate intraclasts.

https://doi.org/10.5194/egusphere-2025-6504
Preprint. Discussion started: 13 January 2026

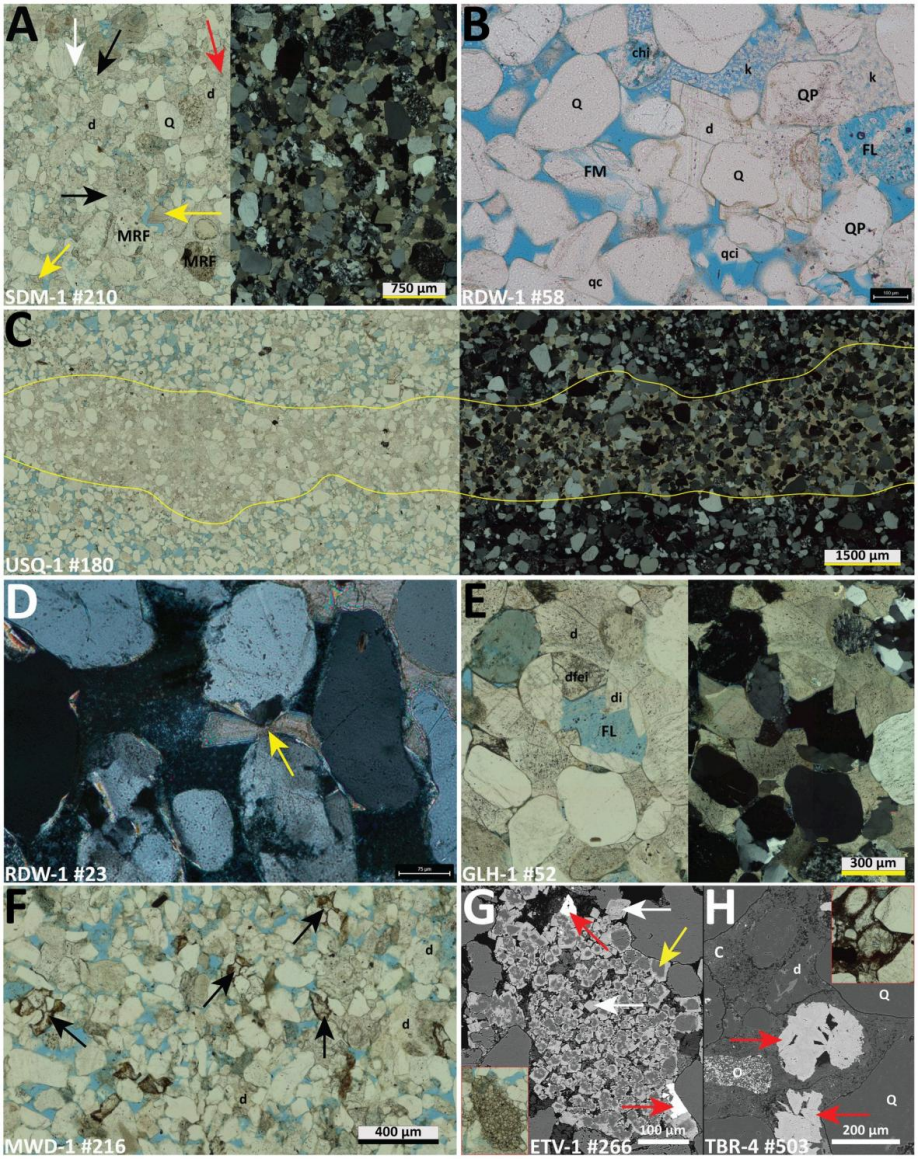

Figure 6: Dolomite and related carbonate types in the Rotliegend sandstones. **A)** Subhedral to anhedral dolomite cement (black arrows) fills intergranular pores and locally inhibits illite rim growth. Isolated or clustered rhombohedral dolomite rhombs (yellow arrows) are typically smaller than surrounding grains. In dolomitized zones lacking grain contacts, dolomite formed prior to major compaction; locally preserved point contacts indicate later growth (red arrow). **B)** Poikilotopic dolomite cement enclosing framework grains. The absence of grain contacts and clean grain surfaces indicate formation prior to major compaction and before other cements. Outward growth into an undeformed, dissolved feldspar (FL) with long grain contacts indicates prolonged carbonate precipitation. **C)** Dolomite cement confined to an isolated wavy lamina (yellow lines). **D)** Deformed dolomite rhomb between detrital grains (yellow arrow), indicating pressure solution of dolomite. **E)** Euhedral dolomite cement growing from intergranular pores into a dissolved feldspar, with the feldspar boundary still visible; part of the intragranular dolomite is Fe-dolomite (dfei). The euhedral habit indicates free growth into pore space. **F)** Rounded or clustered Fe-dolomite rhombs interpreted as sand-sized detrital dolomite grains (black arrows), locally obscured by compaction and pressure dissolution in finer-grained sands. **G)** SEM image of intragranular ankerite rhombs and siderite lozenges. Ankerite forms as overgrowths on dolomite nuclei (yellow arrow); siderite occurs locally as isolated lozenges. The carbonate aggregate is interpreted as detrital. **H)** SEM image of subhedral to euhedral siderite lozenges (red arrows) filling a dissolved grain surrounded by clay cutans (C).

https://doi.org/10.5194/egusphere-2025-6504
Preprint. Discussion started: 13 January 2026

Compositional zonation in dolomite rhombs is common, with SEM images revealing one to several layers in dolomite rims being caused by variable Fe concentrations (Fig. 5B; Fig. 6F-G). The Fe-dolomite primarily forms rims around Fe-poor dolomite crystals, and occasionally occurs as isolated rhombic aggregates in open pore spaces (Fig. 6F). Furthermore, Fe-dolomite is present as a replacive cement in and around the rims of dissolved lithic grains and feldspar, adding to the mineralogical diversity within the sandstones. The Fe-Dolomite content is higher in samples that contain more hematite rich clay coatings, clay grains or dissolved lithics than in other samples. In contrast to dolomite, siderite is uncommon in the samples and occurs as isolated euhedral lozenge shaped rhombs or locally fills intragranular pores together with euhedral opaque cement, as confirmed by SEM analysis (Fig. 6H).

4.2.5 Quartz and Feldspar cement

Quartz cement contents vary throughout the field (1-11%) with the southern cores and the northern cores showing a slight increase in quartz cement content compared to cores from the middle of the field (Table 1). Intergranular quartz cement forms syntaxial, subhedral to euhedral overgrowths around detrital quartz grains (Fig. 8A). The overgrowths are commonly identified by a thin dust rim between the detrital grain and the overgrowth or by the appearance of well-defined euhedral crystal faces (Fig. 8A-B). Small euhedral quartz outgrowths with varying size occur as well. These outgrowths grew perpendicular on the grain rims sometimes in the form of small clusters (Fig. 5C; Fig. 8A). Where dust lines are absent and the quartz cement completely fills intergranular pores, the cement is difficult to distinguish from detrital grains. In these instances, the original grains tend to be recognizable by their slightly more dirty appearance.

Quartz commonly precipitated after the formation of clay coatings and (Fig. 8A), in many cases, before or alongside the development of chlorite. In some samples, it is engulfed by late-stage anhydrite and a second generation of dolomite, whereas in others, it formed later, extensively infilling intragranular pores formed by grain dissolution. Quartz overgrowths predominantly occur where tangential and radial grain-coating illite is absent, poorly developed or discontinuous (Fig. 8A-B). However, it is locally observed in USQ-1 and LNB-1 as anhedral cement encapsulating grains that have a clay coating (Fig. 8C-D). Here, radial illite has not developed, while meshwork illite occupies the remaining intergranular pore space where quartz cement is absent (Fig. 4C). Generally, intragranular euhedral quartz is observed in dissolved grains where it formed from the inner wall of the dissolved grains (Fig. 5C), suggesting continued formation throughout diagenesis. In some samples with relatively high quartz cement content, the quartz cement occupies pore spaces between loosely packed detrital grains that appear texturally floating as well as between grains that exhibit point contacts (Fig. 8A-B). Microcrystalline quartz is only observed in SEM images where it formed locally on grain surfaces or in dissolved feldspar as isolated crystals (Fig. S2C-D). Quartz cement visibly formed nearby chemical compaction of quartz grains by mica, indicating that local chemical compaction processes partially accounted for the formation of quartz cement (Fig. 9F). Feldspar cement is rare in the Groningen area, occurring sporadically as intergranular pore fill. Albite exhibits patchy or microperthitic textures, with ambiguous detrital or authigenic origins in Slochteren sandstones. In rare instances, subhedral to euhedral feldspar crystals formed within dissolved feldspar grains (Fig. 8F).

4.2.6 Sulfate Cements

Anhydrite and barite cements, though minor in content (0-8%), are distinctive authigenic minerals within the Slochteren sandstones. Anhydrite is mainly present as anhedral and blocky intergranular cement commonly associated with dolomite cement. Occasionally it occurs as isolated subhedral or elongated lath shaped crystals in porous sandstones (Fig. 5E; Fig. 9A). Locally, it engulfs and thus postdates dolomite and quartz cement. Two other types of anhydrite are only observed in sandstones from the Ten Boer Member in the northeastern part of the field. The first type occurs as intergranular pore-filling cement (10-18%), often together with detrital clay or dolomite. The second type has a

https://doi.org/10.5194/egusphere-2025-6504
Preprint. Discussion started: 13 January 2026

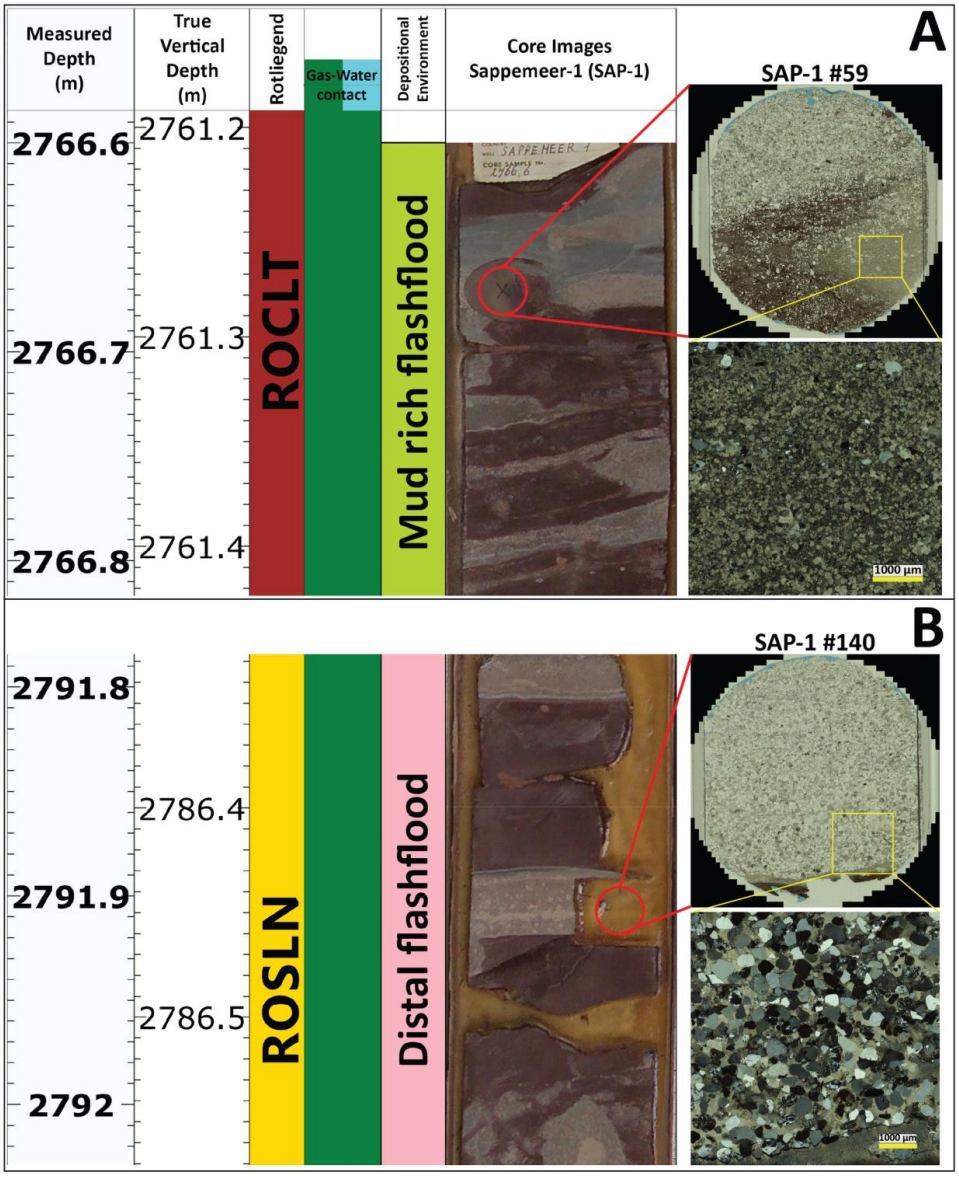

Figure 7: Dolomite cement rich sandstone in a Rotliegend core (SAP-1), which is commonly observed adjacent or close to mudstone intervals. The intercalated thin sandstones represent distal flashflood deposits. The flashflood deposits may either form crevasses deposits, floodplain shales, or thin mouth bar deposits in playa shales. A-B) The dolomite cement supported sandstones have been cemented prior to compaction. Well log data is from the NAM (2020) model, True Vertical Depth (TVD) is based on deviation data from the NLOG website (https://www.nlog.nl/), and calculated by Schlumberger Techlog 2015.3 software. Core images are provided by NAM.

https://doi.org/10.5194/egusphere-2025-6504
Preprint. Discussion started: 13 January 2026

subhedral to euhedral fabric and occurs as part of detrital intraclasts intergrown with barite and euhedral dolomite (Fig. 5E; Fig. 9B). In a few samples, anhydrite has been observed in sedimentary rock fragments as well. Intragranular anhydrite is rarely observed in partially to entirely dissolved grains (Fig. 3A-B). Barite cement is typically present in all wells in minor amounts (0.1-4%). It occurs as isolated euhedral crystals in the intergranular pore space, where it engulfs quartz cement, or as anhedral to subhedral cement in small clusters (Fig. 9A). Moreover, euhedral barite crystals occur in dissolved grains and moldic pores, indicating formation after grain dissolution (Fig. 9D).

4.2.8 Altered and dissolved grains

Dissolution features within the Slochteren sandstones are predominantly observed in feldspar and lithic grains (Fig. 3C; Fig. 4C-D; Fig. 5A-C,G; Fig. 6E) and have been observed in all wells. Dissolution of feldspar typically results in partial to complete removal of the grain interiors, with alteration commonly initiating along cleavage planes or fractures. Replacive cements, such as the distinctive bladed illite, form ghost structures after feldspar cleavage planes (Fig. 4D). The resulting moldic pores from feldspar and lithics are generally undeformed as evidenced by the lack of deformed clay rims. These moldic pores are often filled with quartz, barite, dolomite, kaolinite, and/or chlorite cements, occasionally filling these voids completely (Fig. 5B-C,E). Furthermore, euhedral opaque cement, identified as octahedral pyrite by SEM (Fig. 9E), is locally present in dissolved feldspar, lithics, and intergranular pores.

Lithic grains in the reservoir have undergone significant diagenetic alteration, often obscuring their original composition. Relict outlines of feldspars, ferromagnesian minerals, and lithic fragments are commonly observed, indicating that these grains were often altered to phyllosilicates or developed microporous textures before being fully dissolved during diagenesis. (Fig. 5E,G). Especially, the replacement of volcanic glass, particularly by illite and other clay minerals, is widespread. In metamorphic lithic fragments, feldspars are often fully dissolved, leaving behind voids that preserve the original crystal shapes. Ductile deformation is primarily observed at mudstone clast edges (Fig. 9G), while chemical compaction, also referred to as pressure solution, at grain-to-grain contacts is primarily observed where quartz contacts mica, other quartz grains, feldspar, and carbonate grains (Fig. 6B). This chemical compaction is also observed where tangentially aligned illite is present at point contacts (Fig. 9F,H).

4.3 Regional trends and reservoir quality

4.3.1 Regional versus local variations in authigenic minerals

The studied Slochteren sandstones show distinct regional variations in mineralogical composition (Fig. 10). Correspondence analysis highlights clear interrelationships among authigenic minerals, with wells clustering based on their dominant mineral assemblages. There is a clear distinction between northeastern wells and southern wells, indicating that authigenic mineral assemblages differ systematically across the Groningen field. The northeastern part of the field is characterized by higher contents of illite, chlorite, and illite-smectite, whereas the southern wells and the Annerveen reservoir have a stronger association with kaolinite. However, the Stedum-1 (SDM-1) and Rodewolt-1 (RDW-1) wells in the north, where the Lower Slochteren and Ameland Members are absent (Fig. 1B; Fig. 10A), do not have elevated illite, chlorite, or illite-smectite contents. In contrast, higher contents of these minerals are observed in some samples from the TBR-4 and SAU-1 wells in the western part of the field. Dolomite cement is present in all wells. Its abundance varies significantly, with high dolomite content generally exhibiting a strong negative association with other authigenic minerals. This suggests that dolomite cement prevented the formation of other diagenetic minerals. Quartz cement is present in all wells to some extent and shows an independent distribution compared to the other authigenic minerals, although it has a slightly negative correlation with authigenic clay-rich samples.

https://doi.org/10.5194/egusphere-2025-6504
Preprint. Discussion started: 13 January 2026

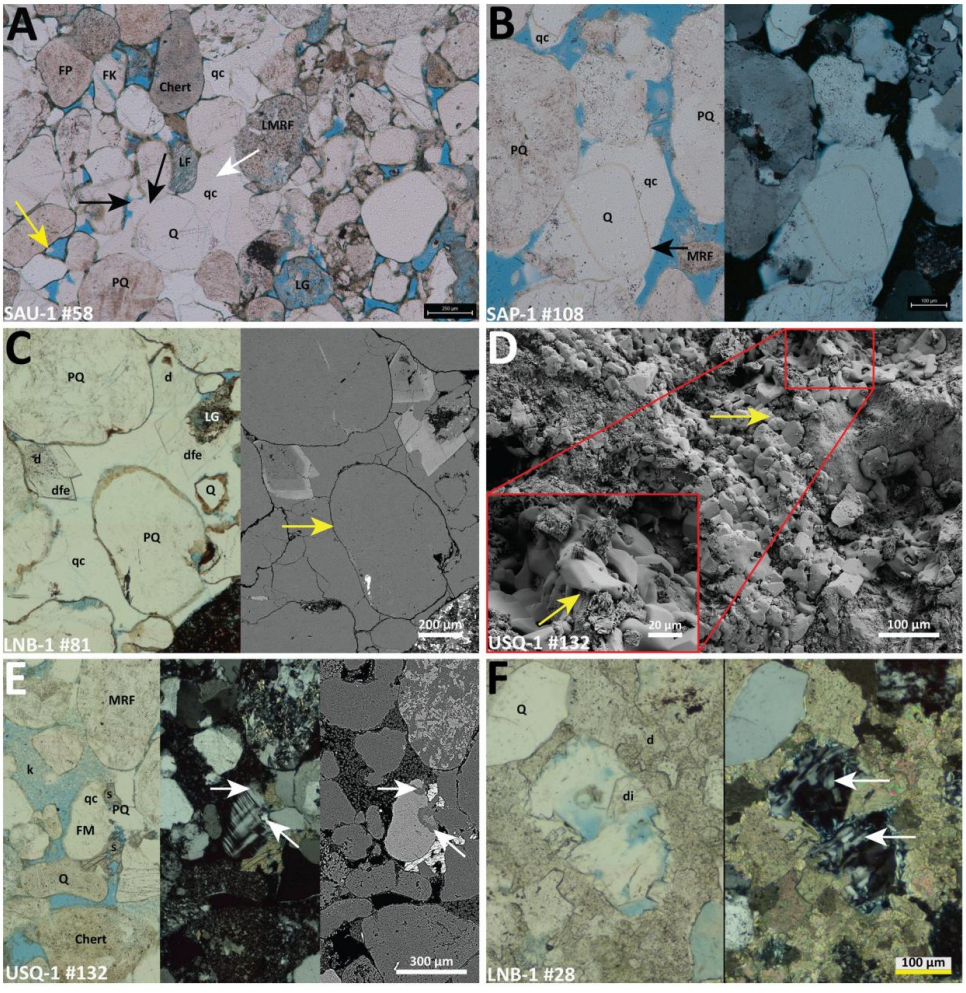

Figure 8: Different types of quartz and feldspar cements in the Rotliegend sandstones. A). Anhedral to subhedral quartz cement (white arrow) is filling the intergranular pore space. Subsequent quartz cement generations (black arrows) formed on top of each other typically on detrital grains where clay rims are absent. Small euhedral quartz overgrowths (yellow arrow) are also typical for the Slochteren sandstones. B) Large euhedral quartz overgrowth that engulfs a detrital quartz grain; left: plain light; right: cross polarized light. C) Quartz cement that engulfs euhedral dolomite/ankerite and entirely fills the remaining pore space. It also encapsulates detrital grains with tangential illite (yellow arrow) and, hence formed later than the clay. D) 3D SEM image with close-up area (red rectangular) of euhedral quartz overgrowths filling the pore space and overgrowing radial illite and chlorite cement (yellow arrow). E) Albite (white arrows) in a microcline grain. F) Intragranular subhedral to euhedral feldspar cement (white arrows) in a dissolved feldspar that is surrounded by dolomite cement.

https://doi.org/10.5194/egusphere-2025-6504
Preprint. Discussion started: 13 January 2026

In addition to the broad regional patterns, strong local deviations in authigenic mineralogy occur both within individual wells and across specific areas of the field. For example, the wells USQ-1, LNB-1, and SAU-1, contain elevated proportions of red tangential clay coatings relative to the colorless tangential illite rims. In the northeastern part of the field, wells USQ-1 and UHM-1 exhibit a minor yet significant occurrence of kaolinite and quartz cement, deviating from the general trend. This indicates that proximal to distal changes of fluvial environment and proximity to the playa alone do not determine the authigenic composition. Furthermore, the occurrence of anhydrite, although minor in abundance, varies slightly across the field. Northeastern wells contain anhydrite solely in the Ten Boer Formation, whereas ETV-1 in the southern part of the field features later-stage anhydrite cement within the Slochteren Sandstone (Table 1), which varies with depth. Furthermore, individual samples can exhibit markedly different authigenic mineral assemblages within a single well with some that are dolomite rich, while others are relatively rich in illite rims and/or kaolinite. These variations underscore that local diagenetic conditions can diverge from regional trends.

4.3.2 Porosity and permeability

Porosity versus Permeability data plots show that there is a correlation between lower porosity and permeability and high dolomite contents in the sandstones (Fig. 10B). Where reservoir quality is high despite dolomite contents exceeding 20%, the preservation of porosity is due to either abundant micropores between dolomite rhombs (Fig. 6A) or localized dolomite-free zones (e.g. in certain laminae) as locally dolomite is confined to certain laminae (Fig. 6C). Most of the samples from the Annerveen and Langebrug reservoirs in the south have low porosities and permeabilities, a relatively higher dolomite content, and lower authigenic clay content compared to samples from the Groningen area. Kaolinite mainly occurs in samples with a higher porosity, although it appears independent from the permeability. Samples with higher illite content show a wide range of porosities and generally lower permeability compared to illite-poor samples. The few exceptions that combine high permeability with high illite content contain only tangential illite and lack radial or meshwork illite. The higher radial and meshwork illite content, locally up to 6%, are thus the key reason why wells in the northeastern part of the field have slightly lower reservoir quality (Fig. 10B). The different influence of the different illite types clearly shows that not only the composition is important for reservoir quality but also the distribution of a mineral within the sediment. Furthermore, sandstones that are relatively rich in illite are poor in quartz cement content, showing a negative correlation. Quartz cement appears not to significantly influence reservoir quality as is shown by the variabilities in porosity and permeabilities.

5. Discussion

5.1 Paragenetic sequence

5.1.1 Early diagenesis

Tangential clay coatings

The authigenic mineral distribution in the Groningen reservoir follows a broadly consistent paragenetic sequence. The earliest diagenetic phase (eodiagenesis), which is influenced by depositional pore waters and near-surface conditions (e.g., oxidic, meteoric) (Morad et al., 2000; Worden and Burley, 2003), is marked by hematite rims, which are consistently enclosed by later cements, a feature typical of continental red beds across the Southern Permian Basin (Gluyas and Leonard, 1995; Schöner and Gaupp, 2005; Busch et al., 2017, 2024). Contemporaneous with hematite formation were the processes that emplaced tangential clay coatings. The prevalence of partially abraded, red-stained coatings throughout the sandstones indicates a significant portion was inherited and transported with the detrital grains, while complete grain-enveloping smectite-illite coatings suggest additional in situ formation (Fig. 3E). Their presence at grain-to-grain contacts provides definitive evidence for a pre-compactional formation (Fig. 3F). This early formation of illite-smectite and chlorite-smectite mixed-clay coatings through illuviation and mechanical infiltration is a ubiquitous feature in Rotliegend fluvio-eolian

https://doi.org/10.5194/egusphere-2025-6504
Preprint. Discussion started: 13 January 2026

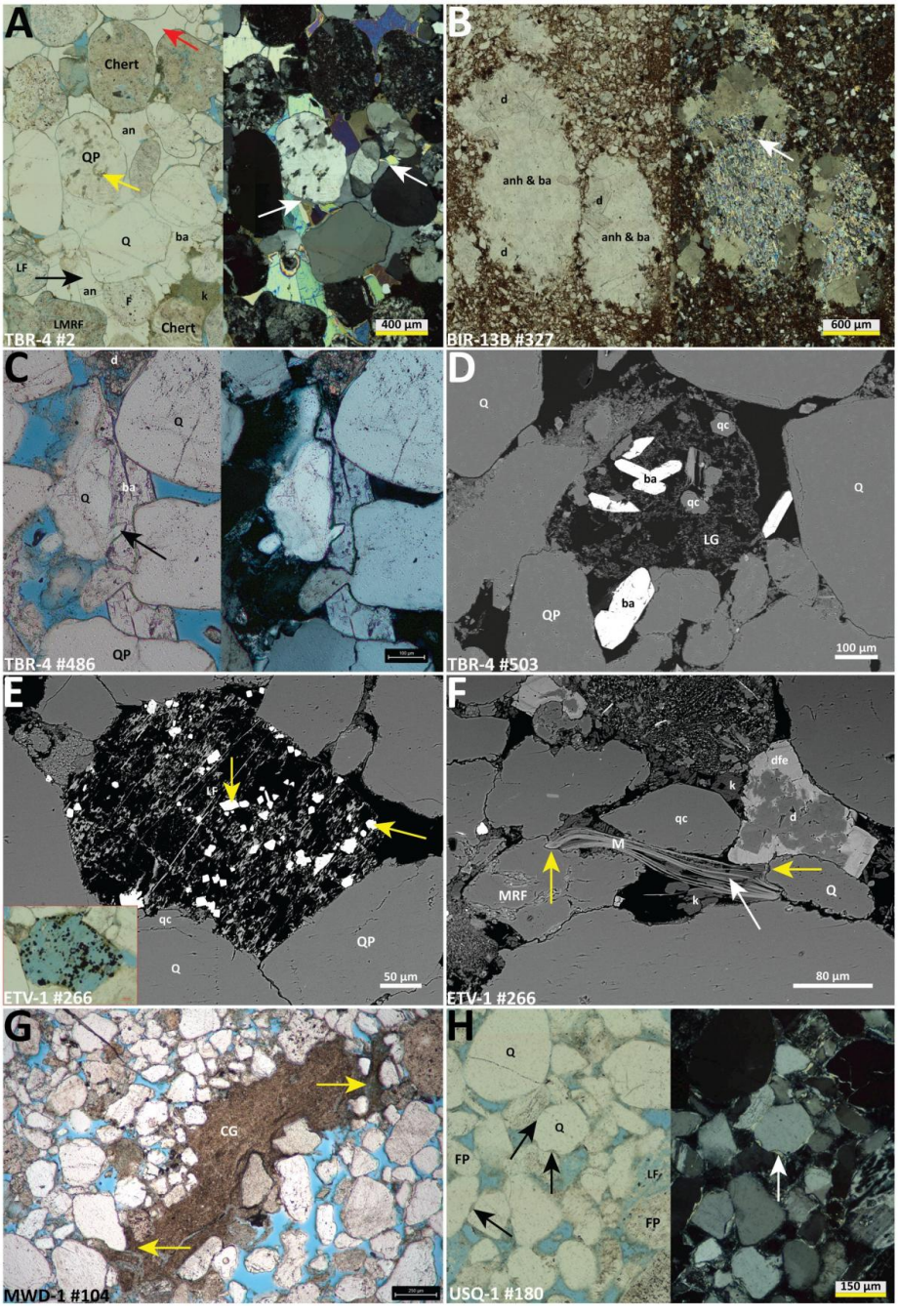

https://doi.org/10.5194/egusphere-2025-6504
Preprint. Discussion started: 13 January 2026

Figure 9: Different types of anhydrite and barite cement, and grain dissolution features in the Rotliegend sandstones. A) Anhedral (red arrow) to euhedral intergranular anhydrite cement (black arrow) formed after barite pore cement (white arrows). The euhedral anhydrite locally forms these elongated crystal laths (black arrow). Quartz grains sometimes contain chlorite 'worms' (yellow arrow), indicating a hydrothermal origin. B) Detrital grains composed of anhydrite (white arrow), barite, and dolomite rhombs. C) Large euhedral barite crystal that formed between the detrital grains. Note that the barite formed on top of, and hence after the quartz overgrowth (black arrow). D) Intragranular isolated, euhedral barite crystals in a dissolved grain and in the adjacent intergranular pore space. E) Typical texture of a feldspar that dissolved along cleavage planes. Note the euhedral opaque cement crystals (yellow arrows), which are only locally observed in the sandstones. F) Quartz chemical dissolution by mica (yellow arrows). G) Ductile clay grain of which the rims (yellow arrows) are deformed and pressed between the detrital grains resembling clay matrix. H) Quartz chemical dissolution adjacent to illite cutans (black and white arrows).

deposits, as documented in numerous studies of Rotliegend sandstones from across the SPB (e.g. Glennie et al., 1978; Purvis, 1992; Lanson et al., 1996; Worden and Morad, 2003; Ziegler, 2006; Esch et al., 2008; Molenaar and Felder, 2018). Furthermore, the absence of hematite in the outer clay coatings suggests formation under non-oxidizing conditions, in contrast to the underlying red clay coatings where hematite is preserved, indicating earlier oxidizing conditions (Molenaar and Felder, 2018; Molenaar et al., 2021). Such non-oxidizing conditions in desert environments can occur in 'pseudogleys', where longer lasting wet conditions take place (Gaupp and Okkerman, 2011; Molenaar et al., 2025).

Early dolomite and anhydrite

A key textural observation within anhydrite-rich sandstones from the Ten Boer Member, and in dolomite-rich intervals across the field, is the presence of floating grain textures where detrital grains are encapsulated by cement. This texture indicates that widespread non-ferroan dolomite and anhydrite cements precipitated as pore-filling, intergranular phases prior to significant mechanical compaction, thereby stabilizing the sediment framework. Dolomite and anhydrite in the Groningen reservoir show a complex paragenesis from syndepositional to deep-burial settings, yet petrographic observations, including detrital carbonate-anhydrite intraclasts and dolomite-supported fabrics, provide definitive evidence for an eodiagenetic origin closely linked to the depositional setting. These intraclasts confirm that dolomite and anhydrite (as gypsum) had already precipitated near-surface and were later reworked, consistent with arid paleosol (e.g. dolocretes, gypscretes) and playa-margin settings (Ziegler, 2006; Gast et al., 2010; Gaupp and Okkerman, 2011; Henares et al., 2014). The fact that dolomite and anhydrite nodules are rimmed by hematite coatings confirms they formed and were oxidized in the vadose zone prior to any reworking. This early phase of carbonate and sulfate cementation is a fundamental characteristic of the Rotliegend, occurring in the realm influenced by depositional pore waters and near-surface conditions, as observed in arid settings (Arakel, 1986; Wright, 1992; Morad et al., 2000) and widely described across the basin (Pye and Krinsley, 1986; Ziegler, 2006; Vincent et al., 2018; Molenaar and Felder, 2019; Miocic et al., 2020; Griffioen et al., 2025). This early cementation, which inhibited the development of tangential clay coatings, was likely driven by evaporation and groundwater table fluctuations in the vadose zone, promoting in situ precipitation (Wright and Tucker, 2009; Amthor and Okkerman, 1998; Molenaar and Felder, 2019). Nodular, poikilitic, and lamina-bound cements, as well as dolomite-rich sandstones near mudstones, further support pedogenic and shallow groundwater origins (Glennie, 1972; McKie and Audretsch, 2005; Stricker and Jones, 2018; Busch et al., 2024). The dolomite-supported fabric in some samples of the Langebrug reservoir implies that similar dolocrete formation processes occurred in the fluvial deposits of this area. In addition, discrete euhedral dolomite rhombs occur within intergranular and pores of relatively porous sandstones. Their isolated occurrence suggests crystallization from early burial fluids that infiltrated the still-open framework after initial near surface eodiagenetic cementation. These rhombs likely formed over a broad range of burial stages, representing a transitional dolomite generation between early dolocretes and later Fe-dolomite. This marks the onset of burial diagenesis, a process often involving the redistribution of

https://doi.org/10.5194/egusphere-2025-6504
Preprint. Discussion started: 13 January 2026

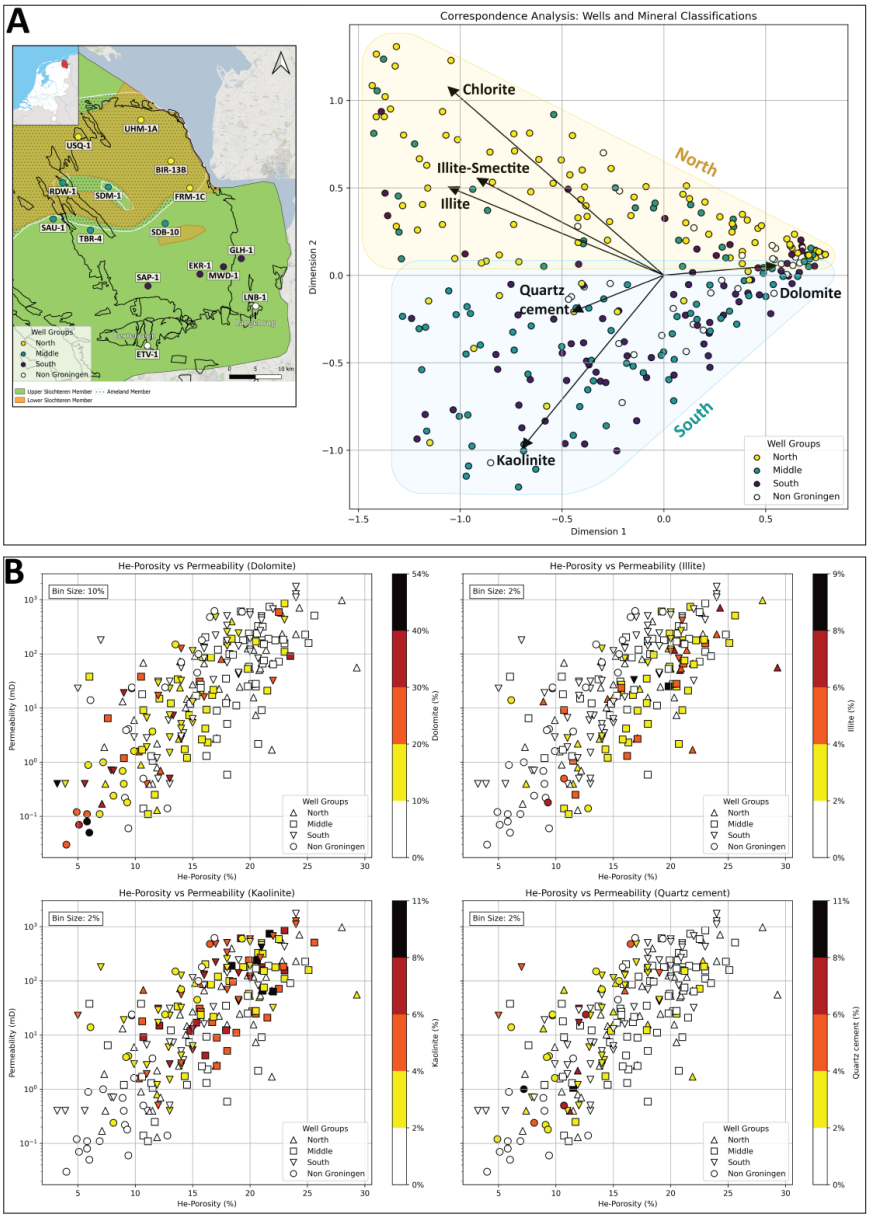

Figure 10: Correspondence analysis and poroperm plots of different authigenic cements. A) Correspondence analysis plot based on point count data showing the correlation between the different authigenic cements in the Rotliegend sandstones and geographic location in the Groningen gas field. The northern wells have relatively more chlorite, illite, and illite-smectite (blue area), while kaolinite is more observed in the southern wells (yellow area). Dolomite has a negative correlation with increasing dolomite content respective to the other authigenic cements. Plotted points between the two areas show a varying content of authigenic minerals with exception of dolomite. B) Poroperm plots of the studied samples showing the correlation between poroperm data and dolomite, illite, kaolinite, and quartz cement. There is no distinct correlation between geographic location and the poroperm data. The poroperm data is from the NLOG website (https://www.nlog.nl/).

https://doi.org/10.5194/egusphere-2025-6504
Preprint. Discussion started: 13 January 2026

earlier cements (Platt, 1994; Molenaar and Felder, 2019), and provided nuclei for subsequent recrystallization during compaction.

5.1.2 Burial and compaction

Compaction

Following the formation of the earliest cements, the Groningen reservoir underwent rapid burial from the Late Permian to the Jurassic, largely due to the deposition of 1-2 km thick Zechstein deposits, reaching maximum depths of approximately 3 km (Fig. 11; Menning et al., 1988; Sindern et al., 2019). Here, pore waters become isolated from surface influence. The most significant phase of porosity reduction occurred during early burial (eodiagenesis to shallow mesodiagenesis) through mechanical compaction, which is most intense within the first 1-2 km of burial (Morad et al., 2000). This process involved two main mechanisms: (1) grain rearrangement, which reorients grains into a tighter packing fabric, and (2) ductile deformation, where soft components like mudstone clasts are plastically deformed between rigid grains (Fig. 9G). Petrographic evidence confirms this progression, with point and long contacts dominating in uncemented sandstones, demonstrating that grain rearrangement was complete. During this early burial stage, and prior to significant grain dissolution or cementation, increasing temperature drove the transformation of early smectitic clay coatings to tangential illite (Folk, 1976; Lanson et al., 1996; Worden and Morad, 2003; Schöner and Gaupp, 2005). The development of concavo-convex contacts indicates deeper burial and the onset of chemical compaction, although the presence of sutured contacts are limited throughout the area. Compaction intensity varied significantly with early lithification; dolomite-rich sandstones retain floating grain textures, proving that early carbonate cement effectively inhibited compaction by stabilizing the framework. Furthermore, carbonate diagenesis progressed during mesodiagenesis, with a next dolomite phase forming poikilotopic and rhombic crystals. The poikilotopic dolomite cement also locally inhibited compaction, suggesting this second phase occurred during burial.

Quartz cement

Quartz cementation commenced after most grain rearrangement, within a compacted framework, and is ubiquitous throughout the reservoir, although its abundance is generally limited and heterogeneous. Its variable timing, predating chlorite and dolomite in some intervals while filling intragranular pores after dissolution in others, demonstrates it was not a discrete event but a continuous process during burial. This is consistent with quartz cementation initiating at temperatures of 70–80 °C and representing a deep-burial, mesodiagenetic process of which the rate of cementation is dependent on silica saturation, temperature and quartz grain surface (Heald and Larese, 1974; Lander et al., 2008; Morad et al., 2010; Ajdukiewicz and Larese, 2012; Busch et al., 2021). Localized quartz cement near chemically compacted quartz grains or micas indicates that chemical compaction, a process well-known to be catalyzed by clay minerals and micas, provided a local silica source (Tada and Siever, 1989; Renard et al. 1997; Bjørkum 1996; Ajdukiewicz and Larese, 2012; Monsees et al., 2020). Evidence for this includes dissolution features at quartz-mica contacts (Fig. 9F, H) and rare sutured quartz grains, particularly where clay-coated detrital grains are in contact. This catalyzing effect of clay and mica-rich intervals on quartz dissolution is well-documented (Bjørkum, 1996; Molenaar et al., 2007; Kristiansen et al., 2011; Monsees et al., 2020). The general rarity of sutured contacts suggests that chemical compaction was not pervasive and limited to discrete zones, potentially inhibited in some intervals by early dolomite cements or the absence of clay coatings and mica at grain contacts. Furthermore, the onset of gas charge and the development of overpressure could have reduced the effectiveness of further chemical compaction by lowering effective stress, thereby terminating key silica-releasing mechanism (Gaupp and Okkerman, 2011; Stricker and Jones, 2018). In deeper intervals, such as wells LNB-1 and USQ-1, quartz cement locally encapsulates clay-coated grains (Fig. 8C-D), demonstrating that at sufficient burial depths and temperatures, quartz overgrowths developed where nucleation surfaces were available (Spötl et al., 1996; Lander et al., 2008; Ajdukiewicz and Larese, 2012). Silica was likely also contributed by the dissolution of K-feldspar (Barclay and Worden, 2000; Worden and Morad, 2000), which is frequently observed throughout the field. However, the released silica from this process

https://doi.org/10.5194/egusphere-2025-6504
Preprint. Discussion started: 13 January 2026

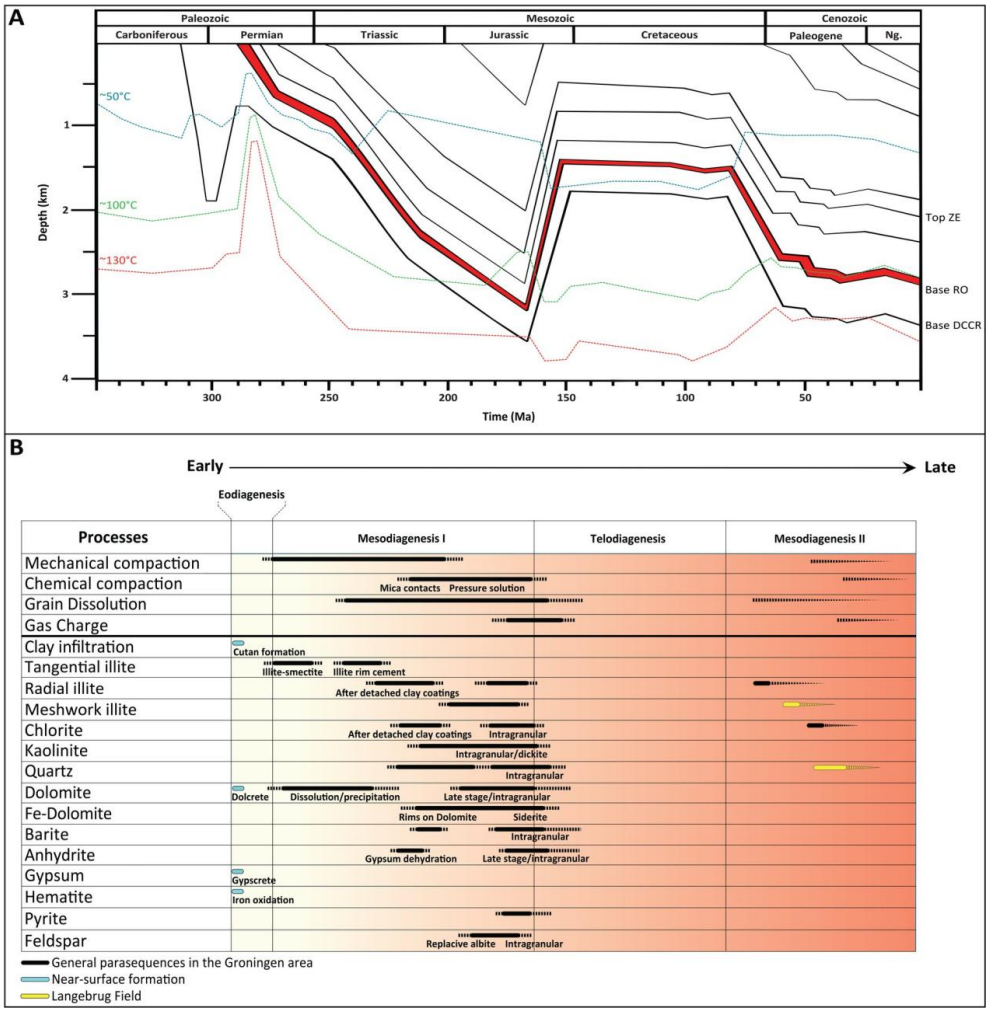

Figure 11: Burial graph and paragenetic sequence of the Groningen area. A) The burial graph and temperature gradients are modified from Bouroullec et al. (2019) based on data from the UHM-2 well, which closely resembles the burial history of DZL-1 (Goldberg et al., 2017). In contrast, the burial graph of ROT-1A, located in the southern part of the gas field, indicates a maximum burial depth approximately 500m shallower both prior to and following uplift (Amberg et al., 2022). The different formations in the figure are Zechstein (ZE), Rotliegend (RO), and Ruurlo (DCCR), which is part of the Limburg Group (Late Carboniferous). B) The paragenetic sequence is based on optical microscopy observations of 310 samples.

primarily resulted in intragranular authigenesis of clay minerals and quartz (Fig. 5A, C, G), creating a competitive sink that limited the silica available for extensive intergranular quartz overgrowths (Molenaar et al., 2025).

590 Radial and meshwork illite and chlorite

The evolution of clay coatings continued with the formation of radial illite and chlorite platelets on tangential illite (Fig. 12), indicating a dual control of precursor availability and burial conditions as observed elsewhere (Gaupp et al., 1993; Worden and Morad, 2003; Dowey et al., 2017; Molenaar et
595 al., 2021). Their absence at grain contacts supports a burial-diagenetic origin. Radial illite and chlorite

https://doi.org/10.5194/egusphere-2025-6504
Preprint. Discussion started: 13 January 2026

observed in the space between grains and detached clay coatings provide evidence that these minerals precipitated after the coatings were locally disrupted by mechanical compaction (Fig. 4A). Radial and meshwork illite are also more common in the north where the Slochteren sandstone (e.g. USQ-1, UHM-1, SAU-1) is slightly deeper than in southern wells, suggesting that prolonged thermal exposure at deeper intervals may have promoted its formation together with the associated playa settings (Fig. 1A; Fig. 10), which influenced the initial pore chemistry of these sandstones. Therefore, this spatial distribution of authigenic illite and chlorite likely reflects a dual control of both depositional facies and burial history. This northern area was dominated by playa lake margin and wet sandflat deposits, which experienced prolonged periods of high groundwater tables and suboxic, alkaline pore waters enriched in Fe^{2+} and Mg^{2+}, enabling the formation of early chlorite precursors and the recrystallization of smectitic clay coatings into illite later during burial (Gaupp et al., 1993; Worden and Morad, 2003; Ziegler, 2006; Gaupp and Okkerman, 2011). This initial pore-water chemistry likely controlled subsequent formation of radial illite and chlorite platelets during further burial.

While radial illite is locally constrained to have formed prior to extensive quartz cementation, as quartz engulfs radial illite (e.g., SDM-1, SAP-1, MWD-1), the exact timing of formation is difficult to determine. Its similar abundance in both the gas and water leg suggests it formed largely before hydrocarbon charge, which would have otherwise inhibited diagenetic reactions. This is consistent with formation during deep burial prior to major Late Jurassic uplift (Lee et al., 1989; Amthor and Okkerman, 1998), likely at temperatures of 60–100 °C (Stricker and Jones, 2018). Support for this model comes from K-Ar illite ages within the SPB, which record at least two distinct phases: one prior to uplift (ca. 150–160 Ma, Late Jurassic), and one during reburial (ca. 70–55 Ma, Late Cretaceous to Early Tertiary) (Turner et al., 1993; Leveille et al., 1997; Gaupp and Okkerman, 2011; Clauer et al., 2012).

A later formation, however, cannot be ruled out as diagenetic reactions can continue in hydrocarbon-saturated sandstones through thin irreducible water films (Taylor et al., 2010). Therefore, illite growth may have continued locally after gas charge, although likely at a reduced rate compared to the water leg. The onset of gas charge may nonetheless have restricted advective fluid flow and thereby limited further illitization, which helps explain the generally low illite abundance in the Groningen field (Leveille et al., 1997; Grecula and Richardson, 2005; Gaupp and Okkerman, 2011). The Late Jurassic to Early Cretaceous uplift and associated cooling could have inhibited illite formation as well, with reservoir temperatures falling from >100 °C to ~50 °C. This contrasts with the deeper (~5000 m) Rotliegend sandstones of the Dutch offshore and northeastern Germany, where hotter, closed-system burial favored extensive late illite formation (Amthor and Okkerman, 1998; Ziegler, 2006).

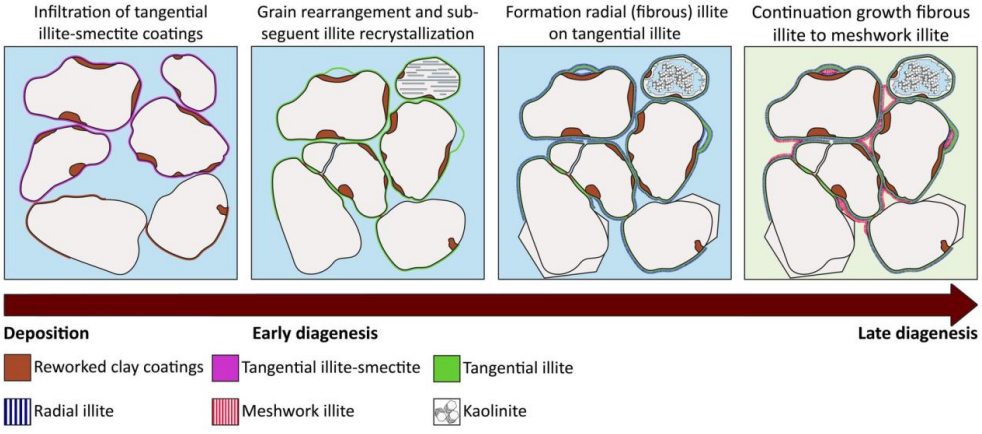

Figure 12: Conceptual model illustrating the diagenetic evolution of clay coatings and the different illite morphologies within the Slochteren sandstones.

https://doi.org/10.5194/egusphere-2025-6504
Preprint. Discussion started: 13 January 2026

A significant body of work on the Southern Permian Basin attributes major illitization events to external fluid influx. Some models propose that potassium for illitization was supplied by Zechstein-derived brines (e.g. Lanson et al., 1996), while others invoke redox-reactions in hydrothermal fluids from the Carboniferous migrating along faults during tectonic events like the Kimmerian Orogeny, leading to rapid precipitation of radial illite and chlorite in conduits (Gaupp et al., 1993; Lee, 1996a,b; Leveille et al., 1997; Lanson et al., 1998). K/Ar dating often links illite growth to such periods of tectonic activity and fluid movement (Lee et al., 1989; Robinson et al., 1993; Zwingmann et al., 1998). The general absence of extensive fibrous illite meshworks, typical of deep faulted parts of the basin (Ziegler, 2006; Gaupp and Okkerman, 2011), and the lack of spatial correlation between illite abundance and fault proximity in the Groningen field, argue against an external fluid source. The position of the Groningen field on a structural high that experienced early gas charge likely shielded it from intense external fluid flow, inhibiting pervasive illitization, a process that has been previously reported in other high fault blocks (Leveille et al., 1997; Gaupp and Okkerman, 2011).

A later phase of intragranular chlorite that fills moldic pores after the dissolution of feldspars and lithics, is interpreted to have been synchronous with or closely followed grain dissolution. The presence of grain rimming chlorite and intragranular chlorite is well-documented in other Rotliegend sandstones (Gaupp et al., 1993; Ziegler, 1993). The prevalence of intragranular chlorite throughout the field is best explained by an internally-sourced model, involving dissolution of volcanic lithics to provide local Fe and Mg (Leveille et al., 1997; Ziegler, 2006; Ajdukiewicz and Larese, 2012; Bello et al., 2024; Griffioen et al., 2025).

Grain dissolution and kaolinite

Grain dissolution commenced along cleavage planes of feldspar and within susceptible lithics, progressing to total grain dissolution after the main phase of mechanical compaction was complete. The resulting pores were subsequently infilled by various late-stage phases such as chlorite, dolomite, quartz, barite and kaolinite, with the latter being dominant and closely following the dissolution of feldspars. It is equally prevalent in dissolved feldspar and in adjacent pores, indicating formation in close proximity to the dissolved grains as observed elsewhere (Lanson et al., 2002; Henares et al., 2014; 2016; Busch et al., 2020). Kaolinite is more prevalent in the central and southern regions, forming as a late-stage diagenetic mineral. This spatial trend does not reflect spatial changes in feldspar dissolution, which is observed in all wells, although it suggests that the geochemical conditions in the northern areas were unfavorable for kaolinite precipitation. The pore water chemistry associated with playa-margin environments likely persisted into progressive burial, buffering the system against the more acidic conditions required for stable kaolinite formation (Lanson et al., 2002; Gaupp and Okkerman, 2011). Grain-rimming kaolinite as described by Waldmann et al. (2016), especially in distal regions close to the basin margin, has not been observed in the Groningen area, potentially due to the widespread pre-existing clay coatings inhibiting grain-rimming kaolinite formation. The illitization of kaolinite, a process requiring a significant potassium source (Lanson et al., 2002; Morad et al., 2010), is petrographically rare and only locally observed. This indicates that the conditions necessary for this reaction were limited, similar to observations in other buried Rotliegend reservoirs (e.g., Turner et al., 1993; Ziegler, 1993; Amthor and Okkerman, 1998). The common presence of kaolinite alongside both tangential and radial illite suggests that both minerals were stable under similar burial conditions in most of the reservoir. The observed vermicular and blocky morphologies suggest multiple formation phases (Purvis, 1992; Ziegler, 2006). The presence of well-crystallised, blocky kaolinite and occasional dickite, as identified in other Rotliegend studies, indicates formation from evolved, acidic fluids. According to established models, CO_2-rich or organic-acid-rich fluids derived from the maturation of organic matter from the Carboniferous are responsible for feldspar alteration and the subsequent precipitation of kaolinite and dickite (Pye and Krinsley, 1986; Ehrenberg, 1991; Platt, 1993). The temperature corresponding to the peak expulsion of these CO_2-rich fluids (~100°C) is compatible with the precipitation temperature of kaolinite and, more especially, dickite (Hunt, 1979; Platt, 1993; Lanson et al., 2002). This is consistent with the occurrence of hydrocarbon-stained kaolinite in wells TBR-4 and ETV-1, suggesting hydrocarbon charge occurred shortly after its formation as previously observed in the Rotliegend (e.g. Gaupp et al., 1993). Locally, the compaction of intragranular kaolinite within

https://doi.org/10.5194/egusphere-2025-6504
Preprint. Discussion started: 13 January 2026

moldic pores indicates that compaction was not fully completed after kaolinite formation. However, moldic pores are generally undeformed, which suggests that their formation post-dated significant compaction.

Burial dolomite and sulfates

Mesodiagenetic dolomite, distinguished from the earlier eodiagenetic phase by its higher iron content, occurs as rims around early dolomite rhombs, within dissolved grains, and as poikilotopic cement. This ferroan dolomite formed progressively during intermediate to deep burial, postdating early carbonate phases and likely representing a continuous solid solution series, consistent with observations across the SPB (Purvis, 1989, 1992; Ziegler, 1993, Ziegler, 2006; Miocic et al., 2020). External acidic and reducing fluids, generated by the thermal maturation of Carboniferous kerogen likely triggered several diagenetic reactions within the Rotliegend, including clay crystallization and carbonate cementation (Vackiner et al., 2013; Goldberg et al., 2017; Sindern et al., 2019). The reducing conditions introduced by migrating hydrocarbons could have favored the formation of Fe-rich cements such as late-stage siderite or pyrite (Fig. 6H; Fig. 9E), consistent with observations in other siliciclastic reservoirs (e.g. Surdam et al., 1993; Parry et al. 2004; Schöner and Gaupp, 2005; Worden, 2006).

The latest diagenetic products include a second generation of anhydrite (e.g. ETV-1, LNB-1, TBR-4), which postdates dolomite and quartz cementation, as well as minor barite. Similar late-stage sulphates have been reported in other Rotliegend reservoirs within the SPB (Gaupp and Okkerman, 2011; Havenith, 2012; Sindern et al., 2019). In the Groningen field, these phases are rare and restricted to isolated samples, suggesting they reflect local redistribution of pre-existing sulphates rather than large scale fluid influx. This contrasts with other Rotliegend settings where fault-bounded juxtaposition of Rotliegend and Zechstein evaporites enabled the influx of sulphate-rich brines, leading to the precipitation of late anhydrite, as demonstrated by isotopic studies (Platt, 1994; Sullivan et al., 1994; Gaupp and Okkerman, 2011; Goldberg et al., 2017). Given that fault throws in the Groningen field are generally <100 m (Buijze et al., 2017), Rotliegend-Zechstein contacts are limited, making external brine migration a minor factor compared to early, facies-controlled diagenetic processes.

5.1.3 Uplift and reburial

Telodiagenesis in the Groningen reservoir was not driven by influx of meteoric waters, as the sequence remained buried to approximately 1500 m depth and was sealed by the Ten Boer Member and Zechstein Formation (Fig. 11). Uplift to shallower depths and lower temperatures (<70-80°C) and a potential influence by hydrocarbon charge likely arrested extensive quartz cementation. However, the formation of authigenic minerals, such as (intragranular) late-stage dolomite, barite, and clays, likely continued, as did grain dissolution to a limited extent. The reburial of the reservoir during the Late Cretaceous to Early Tertiary returned the Slochteren sandstones to depths and temperatures similar to those of the first mesodiagenetic phase (Fig. 11), indicating that further compactional processes where likely constricted to local chemical compaction of detrital grains. Radial illite and locally quartz cementation could have continued to form during this reburial period along with minor grain dissolution (Turner et al., 1993; Leveille et al., 1997; Gaupp and Okkerman, 2011). However, the diagenetic response during this second burial phase was likely subdued as petrographic observations show no evidence of major new cementation events that can be unequivocally attributed to this period. This is consistent with the interpretation that due to the advanced equilibration of detrital material with burial and due to the stabilisation of the grain framework during the first period of burial, the renewed burial had less effect on the Slochteren sandstones (Lee et al., 1989; Gaupp and Okkerman, 2011).

5.2 Effect of authigenic minerals on reservoir quality

Petrographic observations and porosity-permeability data show that dolomite, illite, and kaolinite exert variable impacts on reservoir quality. A strong negative correlation exists between dolomite content and porosity-permeability, demonstrating its pore-occluding effect (Fig. 10B; see also Amthor and Okkerman, 1998; Griffioen et al., 2025). This is most evident in the southern Annerveen and Langebrug

https://doi.org/10.5194/egusphere-2025-6504
Preprint. Discussion started: 13 January 2026

reservoirs, which combine higher dolomite abundances with lower reservoir quality. In some samples, however, porosity is preserved where dolomite is confined to specific laminae or where microporosity persists between rhombs (Fig. 6A, C). Authigenic clays also display mixed effects. Tangential illite coatings are associated with reduced quartz cement volumes, indicating that even partial grain coverage can inhibit quartz overgrowth (Fig. 10B). Kaolinite occurs across a wide porosity-permeability range; while it contributes microporosity, it has little effect on flow capacity. In contrast, radial and meshwork illite, although averaging <2%, locally reduces permeability in northeastern wells by clogging pore throats.

Therse observations suggest that early dolomite cement played a dual role by reducing pore space where pervasive, while stabilizing the grain framework against mechanical compaction where localized, allowing some dolomite-rich sandstones to retain porosity. Illite coatings acted as effective barriers to quartz cementation, making them a critical factor in porosity preservation (Ehrenberg, 1993; Bloch et al., 2002; Gaupp et al., 1993; Ajdukiewicz & Lander, 2010; Molenaar et al., 2021). Kaolinite contributed secondary microporosity, although it had limited influence on permeability as observed in similar siliciclastic settings (Henares et al., 2020; Monsees et al., 2021). The limited development of radial/meshwork illite in Groningen contrasts with more deeply buried Rotliegend reservoirs (Glennie et al., 1978; Leveille et al., 1997; de Jager & Geluk, 2007; de Jager & Visser, 2017). This scarcity likely reflects the field's position as a gas-charged structural high: early gas emplacement created a semi-closed system that reduced effective stress, inhibited compaction, and limited chemical dissolution (Swarbrick & Osborne, 1998; Stricker & Jones, 2018). Consequently, burial diagenesis exerted a relatively minor influence compared to textural controls.

Conclusions

This study establishes a paragenetic framework for the Groningen Rotliegend reservoir, linking authigenic mineral formation to depositional facies, burial history, and reservoir properties. Early diagenesis in near-surface arid settings produced hematite rims, infiltrated and inherited clay coatings, and early dolomite and anhydrite cements that stabilized the framework , while locally occluding porosity. Burial introduced quartz cement, feldspar dissolution, kaolinite, illite, and chlorite, with abundances controlled by depositional setting, precursor availability, temperature, and pore-fluid chemistry. Illite and carbonate cements occur in multiple morphologies and generations, with illite particularly important for inhibiting quartz cement, despite its low abundance. Later uplift and gas charge likely restricted large-scale fluid flow, limiting further cementation, though local influx from overlying Zechstein and Ten Boer, and underlying Carboniferous-fluids were possible.

Eodiagenetic dolomite and anhydrite formed in near-surface arid settings, with dolomite formation continuing during burial with increasing Fe content at depth. Illite and chlorite developed from smectitic precursors, with higher abundances in deeper northern wells, while kaolinite formed mainly in the south through feldspar alteration by acidic fluids. Quartz cementation was spatially heterogeneous, inhibited by clay coatings and later gas charge. Tangential illite inhibited quartz overgrowths while radial illite was volumetrically limited and had negligible effect on reservoir properties. Minor variations in the timing and extent of the authigenic minerals reflect localized differences in diagenetic conditions, such influence of depositional setting and burial.

Diagenetic heterogeneity reflects both regional facies and burial trends as well as local controls such as structural setting, hydrocarbon charge timing, and subtle burial differences. These processes explain why petrophysical models often struggle to capture reservoir variability. Understanding the combined influence of depositional architecture, burial evolution and localized diagenesis is essential for predicting reservoir quality, compaction behavior, and the response of Rotliegend sandstones to future subsurface use.

https://doi.org/10.5194/egusphere-2025-6504
Preprint. Discussion started: 13 January 2026

Competing interests

The authors declare that they have no known competing financial interests or personal relationships that could have appeared to influence the work reported in this paper.

Acknowledgements

We gratefully acknowledge the facility managers J. Huijsmans and Dr. M. Hamers of the scanning electron microscopy (SEM) facilities at Utrecht University (UU) for their assistance and technical expertise, which contributed to the detailed analyses presented in this study. Special thanks go to Dr. R. Wessels for facilitating the Axioscan at the UU, ensuring the highest quality imaging and data acquisition. Furthermore, we sincerely thank W. Smit, R. Stoffers, and the Nederlandse Aardolie Maatschappij (NAM) for their support with sampling of core plug material. Many thanks to EPOS-NL and Dr. R. Pijnenburg for funding the access to the laboratory facilities at UU. This publication is part of a project with file number DEEP.NL.2019.003 of the research programme DeepNL which is financed by the Dutch Research Council (NWO).

Author Credit Statement

S.J. Mulder led the conceptualization of the study, conducted sample collection, laboratory analyses, data visualization, and figure preparation, and drafted the manuscript. J.M. Miocic provided resources, ensured validation of the results, and contributed to writing and editing. M. Felder supported the project by providing comprehensive reviews and editorial input to improve the manuscript.

Data Availability

The datasets generated during the current study are available in the DANS Data Station Physical and Technical Science (https://phys-techsciences.datastations.nl/): https://doi.org/10.17026/PT/DXA7VN. Literature reports provided by NAM are available on request.

References

Aagaard, P., Jahren, J. S., Harstad, A. O., Nilsen, O., & Ramm, M. (2000). Formation of grain-coating chlorite in sandstones. Laboratory synthesized vs. natural occurrences. *Clay minerals*, *35*(1), 261-269.

Ajdukiewicz, J. M., & Lander, R. H. (2010). Sandstone reservoir quality prediction: The state of the art. *American Association of Petroleum Geologists Bulletin*, *94*(8), 1083–1091.

Ajdukiewicz, J. M., Nicholson, P. H., & Esch, W. L. (2010). Prediction of deep reservoir quality using early diagenetic process models in the Jurassic Norphlet Formation, Gulf of Mexico. AAPG bulletin, 94(8), 1189-1227.

Ajdukiewicz, J. M., & Larese, R. E. (2012). How clay grain coats inhibit quartz cement and preserve porosity in deeply buried sandstones: Observations and experiments. *AAPG bulletin*, *96*(11), 2091-2119.

Amberg, S., Back, S., Sachse, V., & Littke, R. (2022). Numerical 3D modeling of burial and temperature history, source rock maturity, and hydrocarbon generation in the onshore northeastern Netherlands. *International Journal of Earth Sciences*, *111*(3), 1033-1055.

Amthor, J. E., & Okkerman, J. (1998). Influence of early diagenesis on reservoir quality of Rotliegende sandstones, northern Netherlands. *AAPG bulletin*, *82*(12), 2246-2265.

Anjos, S. M. C., De Ros, L. F., & Silva, C. M. A. (1999). Chlorite authigenesis and porosity preservation in the Upper Cretaceous marine sandstones of the Santos Basin, offshore eastern Brazil. *Clay mineral cements in sandstones*, 289-316.

https://doi.org/10.5194/egusphere-2025-6504
Preprint. Discussion started: 13 January 2026

Arakel, A. V. (1986). Evolution of calcrete in palaeodrainages of the Lake Napperby area, Central Australia. *Palaeogeography, Palaeoclimatology, Palaeoecology*, *54*(1-4), 283-303.

Barclay, S. A., & Worden, R. H. (2000). Geochemical modelling of diagenetic reactions in a sub-arkosic sandstone. *Clay Minerals*, *35*(1), 57-67.

Becker, I., Wüstefeld, P., Koehrer, B., Felder, M., & Hilgers, C. (2017). Porosity and permeability variations in a tight gas sandstone reservoir analogue, Westphalian D, Lower Saxony Basin, NW Germany: influence of depositional setting and diagenesis. *Journal of petroleum geology*, *40*(4), 363-389.

Bello, A. M., Amao, A., Alqubalee, A., Al-Hashem, M., Albarri, H., Al-Masrahy, M., ... & Babalola, L. (2024). Diagenetic Controls on Reservoir Porosity of Aeolian and Fluvial Deposits: A Case Study from Permo-Carboniferous Sandstones of Saudi Arabia. *Arabian Journal for Science and Engineering*, *49*(1), 973-993.

Bjørkum, P. A. (1996). How important is pressure in causing dissolution of quartz in sandstones? *Journal of sedimentary research*, *66*(1), 147-154.

Bloch, S., Lander, R. H., & Bonnell, L. (2002). Anomalously high porosity and permeability in deeply buried sandstone reservoirs: Origin and predictability. *AAPG bulletin*, *86*(2), 301-328.

Buijze, L., Van Den Bogert, P. A., Wassing, B. B., Orlic, B., & Ten Veen, J. (2017). Fault reactivation mechanisms and dynamic rupture modelling of depletion-induced seismic events in a Rotliegend gas reservoir. *Netherlands Journal of Geosciences*, *96*(5), s131-s148.

Bouroullec, R., Nelskamp, S., Kloppenburg, A., Abdul Fattah, R., Foeken, J., & Ten Veen, J. (2019). Burial and structural analysis of the Dinantian carbonates in the Dutch subsurface. *Report by SCAN*.

Busch, B., Hilgers, C., Gronen, L., & Adelmann, D. (2017). Cementation and structural diagenesis of fluvio-aeolian Rotliegend sandstones, northern England. *Journal of the Geological Society*, *174*(5), 855-868.

Busch, B., Hilgers, C., & Adelmann, D. (2020). Reservoir quality controls on Rotliegend fluvio-aeolian wells in Germany and the Netherlands, Southern Permian Basin–Impact of grain coatings and cements. *Marine and Petroleum Geology*, *112*, 104075.

Busch, B., Okamoto, A., Garbev, K., & Hilgers, C. (2021). Experimental fracture sealing in reservoir sandstones and its relation to rock texture. *Journal of Structural Geology*, *153*, 104447.

Busch, B., Boecker, J., & Hilgers, C. (2024). Improved reservoir quality assessment by evaluating illite grain coatings, quartz cementation, and compaction–Case study from the Buntsandstein, Upper Rhine Graben, Germany. *Geoenergy Science and Engineering*, *241*, 213141.

Clauer, N., Liewig, N., & Zwingmann, H. (2012). Time-constrained illitization in gas-bearing Rotliegende (Permian) sandstones from northern Germany by illite potassium-argon dating. *AAPG bulletin*, *96*(3), 519-543.

Clelland, W.D., Kantorowicz, J.D., Nicolls, C.A., de Weerd, J., & de Gier, F.A.M. (1987) Pilot study into the diagenesis of the northern Groningen wells: Stedum-1, Uithuizermeeden-1 and Delfzijl-1, onshore Netherlands. NAM report RKTR.87.282.

Čyžienė, J., Molenaar, N., & Sliaupa, S. (2006). Clay-induced pressure solution as a Si source for quartz cement in sandstones of the Cambrian Deimena Group. *Geologija*, *53*, 8-21.

https://doi.org/10.5194/egusphere-2025-6504
Preprint. Discussion started: 13 January 2026

Davis, J. C., & Sampson, R. J. (1986). Statistics and data analysis in geology (Vol. 646). New York: Wiley.

Dowey, P. J., Worden, R. H., Utley, J., & Hodgson, D. M. (2017). Sedimentary controls on modern sand grain coat formation. *Sedimentary Geology*, *353*, 46-63.

Ehrenberg, S. N. (1991). Kaolinized, potassium-leached zones at the contacts of the Garn Formation, Haltenbanken, mid-Norwegian continental shelf. *Marine and Petroleum Geology*, *8*(3), 250-269.

Ehrenberg, S. N. (1993). Preservation of anomalously high porosity in deeply buried sandstones by grain-coating chlorite: examples from the Norwegian continental shelf. *AAPG bulletin*, *77*(7), 1260-1286.

Esch, W. L., Ajdukiewicz, J. M., & Reynolds, A. C. (2008, April). Early grain-coat formation in Chaco dune field, New Mexico: insight into formation mechanisms, distribution, and implications for predictive modeling to assist in deep play identification. In *AAPG Annual Convention* (pp. 20-23). AAPG Tulsa, Oklahoma, USA.

Folk, R. L. (1976). Reddening of desert sands; Simpson Desert, NT, Australia. *Journal of Sedimentary Research*, *46*(3), 604-615.

Forbes, G., Soo, D., Smith, M., Reemst, P., & Bueker, C. (2003). Integrated Geological and geophysical Evaluation of the Rotliegend in the Groningen East Area, NAM report NAM200308002107

Fryberger, S. G., Knight, R., Hern, C., Moscariello, A., & Kabel, S. (2011). Rotliegend facies, sedimentary provinces, and stratigraphy, Southern Permian Basin UK and the Netherlands: a review with new observations.

Gast, R.E., Dusar, M., Breitkreuz, C., Gaupp, R., Schneider, J.W., Stemmerik, L., Geluk, M.C., Geißler, M., Kiersnowski, H., Glennie, K.W., Kabel, S. & Jones, N.S. (2010). Rotliegend. In: Doornenbal, J.C. and Stevenson, A.G. (editors): Petroleum Geological Atlas of the Southern Permian Basin Area. EAGE Publications b.v. (Houten), 59-69.

Gaupp, R., & Okkerman, J. A. (2011). Diagenesis and reservoir quality of Rotliegend sandstones in the northern Netherlands—a review.

Gaupp, R., Matter, A., Platt, J., Ramseyer, K., & Walzebuck, J. (1993). Diagenesis and fluid evolution of deeply buried Permian (Rotliegende) gas reservoirs, northwest Germany. *American Association of Petroleum Geologists Bulletin*, *77*(7), 1111–1128.

Geluk, M.C. (2007). Permian. *In*: Wong, Th.E., Batjes, D.A.J. & de Jager, J. (eds): Geology of the Netherlands. Royal Netherlands Academy of Arts and Sciences (Amsterdam): 63– 83.

Glennie, K. W. (1972). Permian Rotliegendes of northwest Europe interpreted in light of modern desert sedimentation studies. *AAPG Bulletin*, *56*(6), 1048-1071.

Glennie, K. W., Mudd, G. C., & Nagtegaal, P. J. C. (1978). Depositional environment and diagenesis of Permian Rotliegendes sandstones in Leman Bank and Sole Pit areas of the UK southern North Sea. *Journal of the Geological Society*, *135*(1), 25-34.

Gluyas, J., & Leonard, A. (1995). Diagenesis of the Rotliegend Sandstone: the answer ain't blowin'in the wind. *Marine and Petroleum Geology*, *12*(5), 491-497.

Goldberg, T., Koenen, M., Nelskamp, S., Vandeweijer, V. (2017). Conceptual diagenetic models for cementation in Rotliegend sandstones. TNO report R10166

Greenacre, M. (2017). Correspondence analysis in practice. chapman and hall/crc.

https://doi.org/10.5194/egusphere-2025-6504
Preprint. Discussion started: 13 January 2026

Griffioen, J., Felder, M., Molenaar, N., Spijker, J., & Hoving, A. (2025). Sediment mineralogy and geochemistry. *Geology of the Netherlands, second edition. Amsterdam University Press (Amsterdam)*, 493-533.

Heald, M. T., & Larese, R. E. (1974). Influence of coatings on quartz cementation. *Journal of Sedimentary Research*, *44*(4), 1269-1274.

Henares, S., Bloemsma, M. R., Donselaar, M. E., Mijnlieff, H. F., Redjosentono, A. E., Veldkamp, H. G., & Weltje, G. J. (2014). The role of detrital anhydrite in diagenesis of aeolian sandstones (Upper Rotliegend, The Netherlands): Implications for reservoir-quality prediction. *Sedimentary Geology*, *314*, 60–74.

Henares, S., Caracciolo, L., Cultrone, G., Fernández, J., & Viseras, C. (2014). The role of diagenesis and depositional facies on pore system evolution in a Triassic outcrop analogue (SE Spain). *Marine and Petroleum Geology*, *51*, 136-151.

Henares, S., Caracciolo, L., Viseras, C., Fernández, J., & Yeste, L. M. (2016). Diagenetic constraints on heterogeneous reservoir quality assessment: A Triassic outcrop analog of meandering fluvial reservoirs. *AAPG Bulletin*, *100*(9), 1377-1398.

van Hulten, F. F. N. (2010). Geological factors effecting compartmentalization of Rotliegend gas fields in the Netherlands. Geological Society, London, Special Publications, 347(1), 301-315.

Hunt, J. M. (1979). Petroleum Geochemistry and Geology: San Francisco, W.H. Freeman, 617 p.

de Jager, J., Doyle, M. A., Grantham, P. J., & Mabillard, J. E. (1996). Hydrocarbon habitat of the West netherlands Basin. In Geology of Gas and Oil under the Netherlands: Selection of papers presented at the 1983 Iternational Conference of the American Association of Petroleum Geologists, held in The Hague (pp. 191-209). Dordrecht: Springer Netherlands.

de Jager, J. (2007). Geological development. *In:* Wong, Th.E., Batjes, D.A.J. & De Jager, J. (eds): Geology of the Netherlands. Royal Netherlands Academy of Arts and Sciences (Amsterdam): 5–26.

de Jager, J., & Visser, C. (2017). Geology of the Groningen field–an overview. *Netherlands Journal of Geosciences*, *96*(5), s3-s15.

Kortekaas, M., & Jaarsma, B. (2017). Improved definition of faults in the Groningen field using seismic attributes. *Netherlands Journal of Geosciences*, *96*(5), s71-s85.

Kristiansen, K., Valtiner, M., Greene, G. W., Boles, J. R., & Israelachvili, J. N. (2011). Pressure solution–The importance of the electrochemical surface potentials. *Geochimica et Cosmochimica Acta*, *75*(22), 6882-6892.

Lander, R. H., Larese, R. E., & Bonnell, L. M. (2008). Toward more accurate quartz cement models: The importance of euhedral versus noneuhedral growth rates. *AAPG bulletin*, *92*(11), 1537-1563.

Lanson, B., Beaufort, D., Berger, G., Baradat, J., & Lacharpagne, J. C. (1996). Illitization of diagenetic kaolinite-to-dickite conversion series; late-stage diagenesis of the Lower Permian Rotliegend Sandstone reservoir, offshore of the Netherlands. *Journal of Sedimentary Research*, *66*(3), 501-518.

Lanson, B., Velde, B., & Meunier, A. (1998). Late-stage diagenesis of illitic clay minerals as seen by decomposition of X-ray diffraction patterns: Contrasted behaviors of sedimentary basins with different burial histories. Clays and Clay Minerals, 46(1), 69-78.

https://doi.org/10.5194/egusphere-2025-6504
Preprint. Discussion started: 13 January 2026

Lanson, B., Beaufort, D., Berger, G., Bauer, A., Cassagnabere, A., & Meunier, A. (2002). Authigenic kaolin and illitic minerals during burial diagenesis of sandstones: a review. *Clay minerals*, *37*(1), 1-22.

Lee, M., Aronson, J. L., and Savin, S. M. (1985). K/Ar dating of time of gas emplacement in Rotliegendes sandstone, Netherlands. *AAPG bulletin*, *69*(9), 1381-1385.

Lee, M., Aronson, J. L., & Savin, S. M. (1989). Timing and Conditions of Permian Rotliegende Sandstone Diagenesis, Southern North Sea: K/Ar and Oxygen Isotopic Data1. *AAPG bulletin*, *73*(2), 195-215.

Lee, M. (1996a). K/Ar dating of illite in understanding fault-related diagenesis (abstract): American Association of Petroleum Geologists, 1996 Annual Convention, Tulsa, Oklahoma, Meeting Abstracts, v. 5, p. 81.

Lee, M. (1996b). 1M(cis) illite as an indicator of hydrothermal activities and its geological implication (abstract): Clay Minerals Society, Annual Meeting 1996, Gatlinburg, Tennessee, Program and Abstracts, p. 106.

Leveille, G. P., Primmer, T. J., Dudley, G., Ellis, D., & Allinson, G. J. (1997). Diagenetic controls on reservoir quality in Permian Rotliegendes sandstones, Jupiter Fields area, southern North Sea. *Geological Society, London, Special Publications*, *123*(1), 105-122.

McBride, E. F. (1989). Quartz cement in sandstones: a review. *Earth-Science Reviews*, *26*(1-3), 69-112.

McKie, T., & Audretsch, P. (2005). Depositional and structural controls on Triassic reservoir performance in the Heron Cluster, ETAP, Central North Sea.

Menning, M., Katzung, G., & Lützner, H. (1988). Magnetostratigraphic investigations in the Rotliegendes (300-252 Ma) of central Europe. *Zeitschrift für geologische Wissenschaften*, *16*(11-12), 1045-1063.

Miocic, J. M., Girard, J. P., Schoener, R., & Gaupp, R. (2020). Mudstone/sandstone ratio control on carbonate cementation and reservoir quality in Upper Permian Rotliegend sandstones, offshore the Netherlands. *Marine and Petroleum Geology*, *115*, 104293

Molenaar, N., Cyziene, J., & Sliaupa, S. (2007). Quartz cementation mechanisms and porosity variation in Baltic Cambrian sandstones. *Sedimentary Geology*, *195*(3-4), 135-159.

Molenaar, N., & Felder, M. (2018). Clay cutans and the origin of illite rim cement: An example from the siliciclastic rotliegend sandstone in the Dutch southern permian basin. Journal of Sedimentary Research, 88(5).

Molenaar, N., & Felder, M. (2019). Origin and distribution of dolomite in Permian rotliegend siliciclastic sandstones (Dutch southern Permian Basin). Journal of Sedimentary Research, 89(10), 1055–1073.

Molenaar, N., Vaznytė, J., Bär, K., & Šliaupa, S. (2021). Illite and chlorite cementation of siliciclastic sandstones influenced by clay grain cutans. Marine and Petroleum Geology, 132, 105234.

Molenaar, N., Hintze, M., & Bär, K. (2025). Detrital composition controlling sandstone diagenesis: the example of the Triassic Bunter sandstone, Germany. *International Journal of Earth Sciences*, 1-18.

Monsees, A. C., Busch, B., Schöner, N., & Hilgers, C. (2020). Rock typing of diagenetically induced heterogeneities–a case study from a deeply-buried clastic Rotliegend reservoir of the Northern German Basin. *Marine and Petroleum Geology*, *113*, 104163.

https://doi.org/10.5194/egusphere-2025-6504
Preprint. Discussion started: 13 January 2026

Monsees, A. C., Busch, B., & Hilgers, C. (2021). Compaction control on diagenesis and reservoir quality development in red bed sandstones: a case study of Permian Rotliegend sandstones. International Journal of Earth Sciences, 110(5), 1683-1711.

Morad, S., Ketzer, J. M., & De Ros, L. F. (2000). Spatial and temporal distribution of diagenetic alterations in siliciclastic rocks: implications for mass transfer in sedimentary basins. *Sedimentology*, *47*, 95-120.

Morad, S., Al-Ramadan, K., Ketzer, J. M., & De Ros, L. F. (2010). The impact of diagenesis on the heterogeneity of sandstone reservoirs: A review of the role of depositional facies and sequence stratigraphy. *AAPG bulletin*, *94*(8), 1267-1309.

NAM (2020). Petrel geological model of the Groningen gas field, the Netherlands. Open access through EPOS-NL. Yoda data publication platform Utrecht University.

Nicholls. C.A. (1987). Sedimentological Description and Facies Definition of Cores from the Rotliegend Group, Groningen/Annerveen Area, North-Eastern Netherlands. NAM report RKTR 87.009

Parry, W. T., Chan, M. A., & Beitler, B. (2004). Chemical bleaching indicates episodes of fluid flow in deformation bands in sandstone. *AAPG bulletin*, *88*(2), 175-191.

Paxton, S. T., Szabo, J. O., Ajdukiewicz, J. M., & Klimentidis, R. E. (2002). Construction of an intergranular volume compaction curve for evaluating and predicting compaction and porosity loss in rigid-grain sandstone reservoirs. *AAPG bulletin*, *86*(12), 2047-2067.

Pettijohn, F. J. (1975). Sedimentary rocks (Vol. 3, p. 628). New York: Harper & Row.

Platt, J. D. (1993). Controls on clay mineral distribution and chemistry in the early Permian Rotliegend of Germany. *Clay minerals*, *28*(3), 393-416.

Platt, J. D. (1994). Geochemical evolution of pore waters in the Rotliegend (Early Permian) of northern Germany. *Marine and Petroleum Geology*, *11*(1), 66-78.

Postma, T., & Jansen, J. D. (2018). The Small Effect of Poroelastic Pressure Transients on Triggering of Production-Induced Earthquakes in the Groningen Natural Gas Field. *Journal of Geophysical Research: Solid Earth*, *123*(1), 401–417.

Purvis, K. (1992). Lower Permian Rotliegend sandstones, southern North Sea: a case study of sandstone diagenesis in evaporite-associated sequences. *Sedimentary Geology*, *77*(3-4), 155-171.

Pye, K., and Krinsley, D. H. (1986). Diagenetic carbonate and evaporite minerals in Rotliegend aeolian sandstones of the southern North Sea: their nature and relationship to secondary porosity development. *Clay Minerals*, *21*(4), 443-457.

Remmelts, G., Nelskamp, S., De Jager, J. & Geluk, M.C. (2025). Petroleum Geology. In: Ten Veen, J.H., Vis, G.-J., De Jager, J. & Wong, Th.E. (eds): Geology of the Netherlands, second edition. Amsterdam University Press (Amsterdam): 535-575.

Renard, F., Ortoleva, P., & Gratier, J. P. (1997). Pressure solution in sandstones: influence of clays and dependence on temperature and stress. *Tectonophysics*, *280*(3-4), 257-266.

Robinson, A. G., Coleman, M. L., & Gluyas, J. G. (1993). The age of illite cement growth, Village fields area, southern North Sea: Evidence from K-Ar ages and 18O/16O ratios. *AAPG bulletin*, *77*(1), 68-80.

https://doi.org/10.5194/egusphere-2025-6504
Preprint. Discussion started: 13 January 2026

Rosera, J. M., & Coleman, D. S. (2022). Correspondence analysis for mineral commodity research: An example workflow for mineralized calderas, southwest United States. *Natural Resources Research*, *31*(1), 9-36.

Schöner, R., & Gaupp, R. (2005). Contrasting red bed diagenesis: the southern and northern margin of the Central European Basin. *International Journal of Earth Sciences*, *94*, 897-916.

Sibley, D. F., & Blatt, H. (1976). Intergranular pressure solution and cementation of the Tuscarora orthoquartzite. *Journal of Sedimentary Research*, *46*(4), 881-896.

Sindern, S., Havenith, V., Gerdes, A., Meyer, F. M., Adelmann, D., & Hellmann, A. (2019). Dating of anatase-forming diagenetic reactions in Rotliegend sandstones of the North German Basin. *International Journal of Earth Sciences*, *108*(4), 1275-1292.

Sissingh, W. (2004). Palaeozoic and Mesozoic igneous activity in the Netherlands: a tectonomagmatic review. Netherlands Journal of Geosciences, 83(2), 113-134.

Spötl, C., Houseknecht, D. W., & Burns, S. J. (1996). Diagenesis of an 'overmature'gas reservoir: the Spiro sand of the Arkoma Basin, USA. *Marine and Petroleum Geology*, *13*(1), 25-40.

Stricker, S., & Jones, S. J. (2018). Enhanced porosity preservation by pore fluid overpressure and chlorite grain coatings in the Triassic Skagerrak, Central Graben, North Sea, UK.

Sullivan, M. D., Haszeldine, R. S., Boyce, A. J., Rogers, G., & Fallick, A. E. (1994). Late anhydrite cements mark basin inversion: isotopic and formation water evidence, Rotliegend Sandstone, North Sea. *Marine and Petroleum Geology*, *11*(1), 46-54.

Surdam, R. C., Jiao, Z. S., & MacGowan, D. B. (1993). Redox reactions involving hydrocarbons and mineral oxidants: A mechanism for significant porosity enhancement in sandstones. *AAPG bulletin*, *77*(9), 1509-1518.

Swarbrick, R. E., & Osborne, M. J. (1998). Mechanisms that generate abnormal pressures: an overview.

Taylor, T. R., Giles, M. R., Hathon, L. A., Diggs, T. N., Braunsdorf, N. R., Birbiglia, G. V., ... & Espejo, I. S. (2010). Sandstone diagenesis and reservoir quality prediction: Models, myths, and reality. *AAPG bulletin*, *94*(8), 1093-1132.

van Thienen-Visser, K., & Breunese, J. N. (2015). Induced seismicity of the Groningen gas field: History and recent developments. Leading Edge, 34(6), 664–671.

Turner, P., Jones, M., Prosser, D. J., Williams, G. D., & Searl, A. (1993). Structural and sedimentological controls on diagenesis in the Ravenspurn North gas reservoir, UK Southern North Sea. In *Geological Society, London, Petroleum Geology Conference Series* (Vol. 4, No. 1, pp. 771-785). The Geological Society of London.

Veen, J., Vis, G. J., de Jager, J., & Wong, T. (2025). Geology of the Netherlands (p. 914). Amsterdam University Press.

Verberne, B. A., Hangx, S. J. T., Pijnenburg, R. P. J., Hamers, M. F., Drury, M. R., & Spiers, C. J. (2021). Drill core from seismically active sandstone gas reservoir yields clues to internal deformation mechanisms. Geology, 49(5), 483–487.

Vincent, B., Waters, J., Witkowski, F., Daniau, G., Oxtoby, N., Crowley, S., & Ellam, R. (2018). Diagenesis of Rotliegend sandstone reservoirs (offshore Netherlands): The origin and impact of dolomite cements. *Sedimentary Geology*, *373*, 272-291.

https://doi.org/10.5194/egusphere-2025-6504
Preprint. Discussion started: 13 January 2026

Walderhaug, O., & Bjørkum, P. A. (2003). The effect of stylolite spacing on quartz cementation in the Lower Jurassic Stø Formation, southern Barents Sea. *Journal of sedimentary research*, *73*(2), 146-156.

Waldmann, S., & Gaupp, R. (2016). Grain-rimming kaolinite in Permian Rotliegend reservoir rocks. Sedimentary Geology, 335, 17-33.

Worden, R. H., & Burley, S. D. (2003). Sandstone diagenesis: the evolution of sand to stone. *Sandstone diagenesis: Recent and ancient*, 1-44.

Worden, R. H., & Morad, S. (2003). Clay Mineral Cements in Sandstones.

Worden, R. H. (2006). Dawsonite cement in the Triassic Lam Formation, Shabwa Basin, Yemen: A natural analogue for a potential mineral product of subsurface CO_2 storage for greenhouse gas reduction. *Mar. Petroleum Geol.* 23 (1), 61–77.

Worden, R. H., Armitage, P. J., Butcher, A. R., Churchill, J. M., Csoma, A. E., Hollis, C., Lander, R. H., & Omma, J. E. (2018). Petroleum reservoir quality prediction: overview and contrasting approaches from sandstone and carbonate communities.

Wright, V. P. (1992). Paleosol recognition: a guide to early diagenesis in terrestrial settings. In *Developments in Sedimentology* (Vol. 47, pp. 591-619). Elsevier.

Wright, V. P., & Tucker, M. E. (Eds.). (2009). *Calcretes*. John Wiley & Sons.

Ziegler, P. A. (1975). The geological evolution of the North Sea area in the tectonic framework of North Western Europe.

Ziegler, K. (2006). Clay minerals of the Permian Rotliegend Group in the North Sea and adjacent areas. *Clay Minerals*, *41*(1), 355–393.

Zwingmann, H., Clauer, N., & Gaupp, R. (1998). Timing of fluid flow in a sandstone reservoir of the north German Rotliegend (Permian) by K-Ar dating of related hydrothermal illite. *Geological Society, London, Special Publications*, *144*(1), 91-106.